Finescale Structure and Microphysics of Coastal Stratus

GABOR VALI, ROBERT D. KELLY, JEFFREY FRENCH, SAMUEL HAIMOV, AND DAVID LEON

Department of Atmospheric Science, University of Wyoming, Laramie, Wyoming

ROBERT E. MCINTOSH AND ANDREW PAZMANY

Microwave Remote Sensing Laboratory, University of Massachusetts, Amherst, Amherst, Massachusetts

(Manuscript received 24 April 1997, in final form 29 January 1998)

ABSTRACT

Observations were made of unbroken marine stratus off the coast of Oregon using the combined capabilities of in situ probes and a 95-GHz radar mounted on an aircraft. Reflectivity and Doppler velocity measurements were obtained in vertical and horizontal planes that extend from the flight lines. Data from three consecutive days were used to examine echo structure and microphysics characteristics. The clouds appeared horizontally homogeneous and light drizzle reached the surface in all three cases.

Radar reflectivity is dominated by drizzle drops over the lower two-thirds to four-fifths of the clouds and by cloud droplets above that. Cells with above-average drizzle concentrations exist in all cases and exhibit a large range of sizes. The cells have irregular horizontal cross sections but occur with a dominant spacing that is roughly 1.2–1.5 times the depth of the cloud layer. Doppler velocities in the vertical are downward in all but a very small fraction of the cloud volumes. The cross correlation between reflectivity and vertical Doppler velocity changes sign at or below the midpoint of the cloud, indicating that in the upper parts of the clouds above-average reflectivities are associated with smaller downward velocities. This correlation and related observations are interpreted as the combined results of upward transport of drizzle drops and of downward motion of regions diluted by entrainment. The in situ measurements support these conclusions.

1. Introduction

Understanding the evolution of drizzle in stratus is hindered by a number of difficulties in spite of the apparent simplicity of these clouds. The characteristic vertical profiles and near-adiabatic values of the liquid water content (LWC) tend to indicate that vertical transport is taking place. However, it is also clear that this is not accomplished with major organized updrafts so that Lagrangian models of condensation and coalescence are inapplicable. The question is to what extent and on what scales vertical motions and drizzle development are random versus organized.

Model calculations have been devised that superimpose some form of turbulent transport on the coalescence process (Nicholls 1987; Baker 1993; Austin et al. 1995; Feingold et al. 1996). In these models, the main focus is on the vertical distribution of cloud properties, and they are anchored to observations in terms of the variance of vertical air velocities measured by aircraft. On the other end of the scale, Paluch and Lenschow (1991) showed evidence for variations over horizontal scales of >10 km in cooling by evaporation of drizzle; similar patterns are also apparent in the data of Austin et al. (1995). Cellular patterns of drizzle formation with scales on the order of 1 km are incorporated, due to quite different forcing, in the model results of Kogan et al. (1995) and of Feingold et al. (1996). The role of gravity waves above the cloud layer in imposing local variations that ultimately also influence drizzle development has been mentioned by a number of authors. Internal circulations are also assumed to play a role in the eventual breakup of stratus to stratocumulus (e.g., Schubert et al. 1979; Krueger et al. 1995a,b).

A large number of investigations have shown the existence of structure (inhomogeneities) in the internal composition, thermodynamic and turbulence characteristics, and radiative properties of stratus and stratocumulus (e.g., Sauvageot 1976; Paluch and Lenschow 1991; Welch et al. 1988a; Welch et al. 1988b; Lee et al. 1994; Boers et al. 1988; Cahalan and Snider 1989; Duroure and Guillemet 1990; Kikuchi et al. 1991; Kikuchi et al. 1993; Gollmer et al. 1995; Davis et al. 1996; Gerber 1996). However, the connections between these patterns and the development and spatial distribution of

Corresponding author address: Gabor Vali, Department of Atmospheric Science, University of Wyoming, Box 3038, Laramie, WY 82071. E-mail: vali@uwyo.edu

drizzle were largely inaccessible. This contrasts with the extensive studies available on the structure of precipitation from a variety of other precipitation types (Fabry 1996, and references therein).

One of the difficulties in studying the connection between structure in other characteristics and drizzle development is that cloud composition, specifically the size distribution of cloud droplets and drizzle drops, is poorly documented by the in situ probes carried on aircraft. Total cloud droplet concentration and liquid water content are the only parameters for which adequate sample sizes can be obtained; the resolution achievable in measurements of the concentrations of larger droplets and of drizzle drops is very limited. A common limitation for all in situ measurements is that they are restricted to a line along the flight path. Liquid water path (LWP) measurements via microwave radiometry provide another type of description (e.g., Cahalan and Snider 1989), but because of the inherent vertical integration through the entire depth of the clouds these data are also difficult to interpret from the point of view of cloud spectra evolution. The purpose of this paper is to show observations obtained with an airborne radar operating at 95 GHz (3-mm wavelength) in marine stratus, and to explore the additional insights these data can provide on cloud processes. While still an integrative quantity whose precise interpretation depends on knowledge of the size distribution of drops, radar reflectivity is unique in depicting the spatial distribution of the relative intensity of precipitation formation. The information obtained from the radar-observed velocity fields is also unique in depicting essentially instantaneous fields of hydrometeor velocities over regions of several kilometers in horizontal extent. A further strength of the airborne radar data used in these studies is that the reflectivity and Doppler velocity data are referenced along the flight path to information derived from the in situ probes carried by the aircraft.

The observations to be described were made off the Oregon coast in September 1995. Flight locations were generally 30–80 km off the coast, in the vicinity of 45°N lat and 124°W long. A total of 11 flights were made over a period of three weeks. The boundary layer was less than 1 km deep in all cases and cloud depths varied from 100 to 400 m. Flight patterns consisted of mixtures of level segments below and within the cloud, and of vertical soundings along straight or spiral paths. The duration of each flight was 2–4 h, and the cloud area explored was about 50 km in horizontal extent. Data from three consecutive days will be presented. One of these days had quite unusual dynamic and thermodynamic structures, whereas the other two days were more typical of marine stratus and stratocumulus situations. The contrasts and similarities that were found in the data for these different situations are helpful in isolating physical links and in establishing the generality of some of the findings.

The main focus of the paper is on the development of drizzle. However, this interest is not interpreted narrowly; cloud characteristics are presented in some detail so that these observations, and the potential applicability of the unique radar observations to those from other areas can be assessed.

2. Instrumentation

a. In situ probes

The University of Wyoming King Air aircraft is equipped for the measurement of position, attitude, relative air motion, hydrometeor distributions, and radiation. Specifications of the instrumentation relevant to this study are listed in Vali et al. (1995). To clarify the interpretation of the data presented here, some comments on the measurement of key parameters are in order.

As will be seen in the soundings, humidity measurements just above the cloud layer appear somewhat anomalous, showing constant values or increases rather than decreases. Humidity measurements are available from two instruments: a chilled-mirror device and an infrared absorption device. Although not in perfect agreement, both devices show the same trends above the clouds. The observed profiles are independent of whether the data were recorded during ascents or descents. Thus, since the two instruments are located at different positions on the aircraft and operate on different principles, and since prewetting in the clouds does not seem to influence the results, we have no reason at this time to question the humidity measurements.

Vertical wind is determined with data from an inertial navigation system and from a gust probe, which are recorded at 50 Hz after antialias filtering with a cutoff frequency of 10 Hz. Instantaneous vertical wind values have a precision of the order of cm s^{-1}. Average vertical winds for wavelengths of 100 m to 5 km are limited in accuracy by the determination of aircraft motion from the inertial reference system and the gust probe; the resultant error is estimated to be <1 m s^{-1}. In any event, mean vertical velocities over kilometer distances are forced to zero.

Cloud droplets are measured with the forward-scattering spectrometer probe (FSSP, from Particle Measuring Systems, Inc.) in 15 size categories. Most data for this paper were recorded with bin sizes of 3 μm at 10 Hz. Calibration of the FSSP is based on sizing of polystyrene spheres; the sample volume is determined from the laser beam diameter and from a micrometer tracing of the depth of field. Data processing follows Brenguier and Almodei (1989) and Brenguier (1989). The ''reset'' rate was not recorded for this project, so it was set to five times the ''strobe'' rate; later data on the reset parameter proved that assumption to be valid. Although no reference standards are available, we estimate the accuracy of total droplet concentrations to be around 10%, with sizing accuracy around 15%. These

errors lead to roughly a factor 1.7 maximum possible uncertainty in the LWC derived by integration of the droplet spectra. Actual errors are probably smaller; comparisons with LWC values measured with the Commonwealth Scientific and Industrial Research Organisation (CSIRO) hot-wire probe generally show agreement within about 20%. Paluch et al. (1996) estimate the inherent errors in LWC derived from the FSSP data to be $\pm 13\%$.

Drizzle drops are measured with an optical array probe (2D-C, from Particle Measuring Systems, Inc.). Measurement granularity is 25 μm; data for this study were grouped into intervals of 50–100, 100–150, 150–200, 200–250, and 250–350 μm. No drops beyond 350-μm diameter were observed in this study. Artifacts due to water streaming from the probe tips were rare, but were nonetheless removed in processing. Drop sizes were taken to be given by their maximum dimensions along the flight direction; this treatment leads to a possible underestimation of drop size by about 25 μm due to the electronic delay in triggering the detector circuits. No corrections were made for the size dependence of the depth of field. This is based on agreement found between the size distributions of ice crystals measured by direct collection and by the 2D-C probe. Baumgardner and Korolev (1997) show that for water drops, and with the response time of the detectors taken into account, the depth of field for drops <100 μm is underestimated; for our first size category their correction would be approximately a factor of 10. The aforementioned shortcomings in data processing may be responsible for the local minima in our size spectra near 50-μm diameter, but we do not consider the evidence for this conclusive.

b. Radar

The advantages and disadvantages of 95 GHz (3-mm wavelength) radars for meteorological studies have been widely discussed. Lhermitte (1988a,b) reported the first meteorological applications of this frequency. Pazmany et al. (1994a), Vali et al. (1995), and Galloway et al. (1996) describe the results of work done by the University of Massachusetts and University of Wyoming groups with earlier versions of the radar system utilized in this study. Clothiaux et al. (1995) presented a summary of results obtained by the Pennsylvania State University group in various cloud types. Sassen and Liao (1996) presented calculations of reflectivity and cloud content for 95 GHz. Considerable interest in 95-GHz radars derives from plans to build a spaceborne radar of this wavelength (Browning et al. 1993; IGPO 1994).

From our point of view, the choice of the 95-GHz frequency was dictated by the small overall size and by the narrow beam angle achievable with a small antenna, enabling such a radar to be fitted at reasonable cost to the University of Wyoming twin-engine King Air aircraft. The radar used in this study has been described in Mead et al. (1994) and in Pazmany et al. (1994b). Main parameters of the radar, as used in these experiments, are 1.6-kW peak power, 30 m range resolution, 10–20 kHz pulse repetition frequency, real-time integration of up to 500 pulses, 7.5–15 km and 8–16 m s^{-1} unambiguous distance and velocity ranges, 60 m minimum range.

The antenna is pointed to the right side of the fuselage. A reflector plate housed in an airfoil faring outside the fuselage can be moved into position to direct the beam vertically upward. The half-power beam angle is 0.7°. The antenna and reflector combination were designed to point either vertically up when the aircraft is in level flight at average load and airspeed, or perpendicular to the longitudinal axis, to the right of the aircraft. For reflectivity data we do not correct the locations of range bins for small deviations ($<5°$) in pitch or in yaw. The measured Doppler velocities are converted to ground-relative values by removal of components of the aircraft motion in the beam direction. The manner in which this was accomplished is described in Leon and Vali (1998). In addition, during the Oregon program the aircraft was flown over the NOAA Ka-band radar (Kropfli et al. 1995) and the vertical Doppler velocities compared; based on that, a -0.3 m s^{-1} correction was applied to the airborne vertical Doppler velocity data presented in this paper.

The received power measurement was calibrated on the ground using a corner reflector. The accuracy of the calibration is ± 2 dB. During operation, the power output of the radar was monitored and found to have been repeatable within 3.6 dB over the 3 days discussed in this paper. The receiver noise level was constant to better than 1 dB during this same period. Over periods of several minutes, the data collection interval for images to be presented here, both the transmitter and the receiver were steady to better than 5% coefficient of variation. Thus, the precision of reflectivity values within individual data segments (images) is quite high, but absolute values have, conservatively, possible errors of up to 5 dB.

Reflectivities have been thresholded to exceed the fluctuation in noise level by at least two standard deviations. Noise levels were determined from power received just prior to transmission of pulses. Received reflectivity values below the threshold were set to large negative numbers and appear in the images as black areas; also, no velocity data are accepted for such points. The contribution of turbulence to the observed reflectivities is estimated to be negligible. Using the observations reported by White et al. (1996), the calculated reflectivity factors for turbulence are near -80 dBZ. Attenuation at 95 GHz is appreciable for clouds of the type encountered in this work. From data collected with a horizontal beam in cloud areas indicated by the in situ probes to be relatively uniform, we determined that the attenuation coefficient (in dB km^{-1}) is well represented

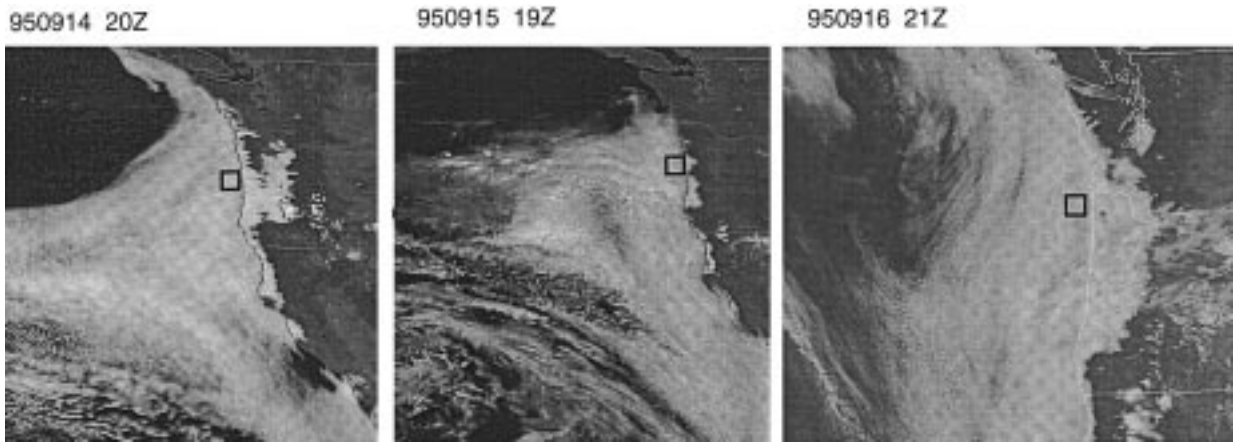

FIG. 1. Satellite images (visible channel) of area along coasts of southern Washington, Oregon, and northern California for the three study periods. Images are from *GOES-7* for 14 and 15 September 1995, and from *NOAA-14* for 16 September 1995. Areas covered by aircraft flights are outlined with boxes.

by the relation [0.7 + 4.4 (LWC)], where LWC is in g m^{-3}. This result agrees well with the calculated values of Liebe et al. (1989) and Lhermitte (1990). Attenuation corrections were made for horizontal echo sections based on the above formula and on the mean LWC measured during the period. Attenuation corrections were not made for vertical cross sections, since the combination of limited cloud depth and small LWC values leads to maximum attenuations of <1 dB, as also shown by the calculations of Clothiaux et al. (1995).

3. General cloud characteristics

All 3 days to be discussed had solid cloud covers without visible breaks in the clouds. Therefore, the cases are classified as stratus, not stratocumulus. Satellite images for the three study periods are shown in Fig. 1. As the small squares indicate, the flight locations were 30–80 km off the coast, in clouds of uniform appearance, and at distances from cloud boundaries that provided a minimum of 12 h of advection time to the region of observation. The images also show that the flight areas were to the NE of large regions of stratocumulus. The flights took place near local noon. No clouds were present above the stratus, so the clouds were exposed to full solar heating and infrared cooling.

The depth of the boundary layer gradually thickened during the 3-day sequence to be described in detail (14–16 September 1995), and there were significant changes over that period in winds and in sea surface temperatures. On the day preceding the sequence (13 September) the base of the inversion was at 300 m above sea level[1] and the stratus layer was about 150 m in depth. On the first study day the inversion base was at 550 m. By the last day (16 September) the inversion base was at 920 m and cloud depth increased to 300 m. For comparison, the cloud at the beginning of the first Lagrangian experiment (L1) described by Bretherton and Pincus (1995) was at similar altitude, and was about as deep as the cloud observed on the second day of our sequence. In this paper, the evolution of the cloud layer is not analyzed in terms of large-scale meteorological factors. Cloud observations for each day are treated essentially as independent datasets. This is justified by the brevity of observations on each day in comparison with the time interval between them. Nonetheless, by focusing on three consecutive days in this paper, an example is provided of the longer-term evolution of the boundary layer and of the associated stratus.

Soundings for the three study days (designated 950914 through 950916) are shown in Fig. 2. Panels (from left to right) show data for temperature (T), total mixing ratio (q_t), equivalent potential temperature (θ_E), potential temperature (θ), horizontal wind direction (wdir), and horizontal wind magnitude (wmag). Data in these plots are averages in 25-m altitude blocks over all observations from arrival at the study site to departure from it roughly 2 h later. The depths of the cloud layers are indicated by heavy vertical lines in the first panel of each sounding. Temperature profiles are not far from $T = 15°C - 0.005H$, with H in meters, between 330 m and cloud top for 950914, and for the entire layer below the inversion for the other two days. This is near the wet-adiabatic lapse rate for 10°C and 950 mb. Temperature changes at the inversion remained roughly the same, +5°C, for the period. Fluctuations in temperature at any given altitude were quite small (typically <0.2°C standard deviation) over the typical 2-h duration and about 50-km spatial extension of each flight. Below the inversion the standard deviations of the temperature measurements were ≈ 0.2°C. Greater variability was found near the inversion layer. Humidity measurements

[1] All heights in this paper are referenced to sea level. Altitude data were taken from a precision radar altimeter.

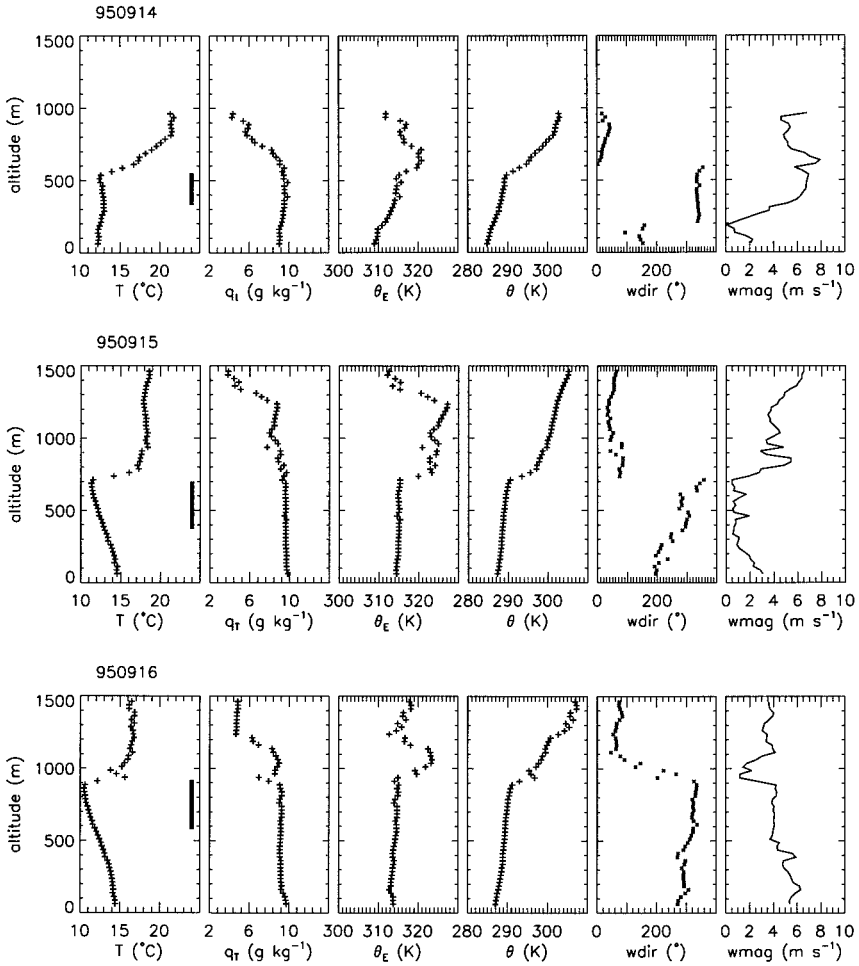

FIG. 2. Vertical profiles of temperature (T, °C), total specific humidity (q_t, g kg^{-1}), equivalent potential temperature (θ_E, K), potential temperature (θ, K), wind direction (wdir, °true), and wind speed (wmag, m s^{-1}). The data include approach and departure soundings into and out of the study area and all data from within the study area. Data are plotted as averages over 25-m height intervals. Heavy lines in the temperature panels indicate the vertical extents of the clouds: (a) 14 September 1995 (950914), (b) 15 September 1995 (950915), and (c) 16 September 1995 (950916).

show unusual constancy just above the cloud layers instead of the more usual sharp decrease; as discussed in section 2, we have no reason to doubt the validity of these data. [A humidity sounding similar to those we observed was also reported by Rogers and Telford (1986) in their sounding S2, which was, coincidentally, taken closest to the coast.] In all cases, within the accuracy of the measurements, saturated conditions prevailed to the lowest flight altitudes (~50 m). The principal stratification of the boundary layer, based on detailed temperature profiles, is given in Table 1.

TABLE 1. Stratification by stability.

Date	Height interval (m)	Lapse rate (°C km^{-1})
14 Sep 1995	0–330	+3.2
	330–520	−5.0
15 Sep 1995	0–700	−5.0
16 Sep 1995	0–100	−7.9
	100–300	−1.0
	300–580	−8.0
	580–920	−5.0

As shown in Fig. 2 and in Table 1, the sounding for 14 September (950914) has several unusual features that deserve closer examination. Temperature and humidity soundings are shown in greater detail in Fig. 3; points in this diagram represent 1-s averages of data recorded during several ascents and descents through the cloud layer. The humidity measurements here show increases above the cloud layer; in Fig. 2 these are less evident due to the larger scale of the diagram and because of the averaging by altitude intervals. The main cloud layer, defined (somewhat arbitrarily) as the region of near-constant θ_E values, overlies a stable layer of about 330-

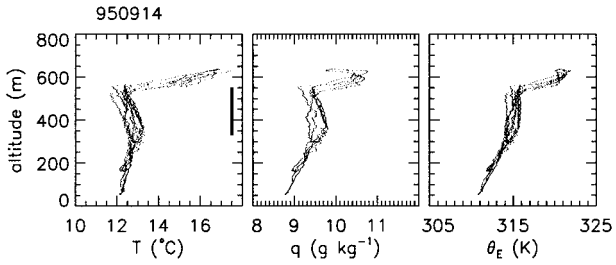

FIG. 3. Detailed data for temperature (T, °C), specific humidity (q, g kg^{-1}), and equivalent potential temperature (θ_E, K) from a series of ascents and descents through the cloud on 14 September 1995. Each point represents 1 s of data. Cloud depth is indicated by the heavy vertical line in the first panel. Points within the main cloud layer (330–550 m) lie along slightly different, but constant, θ_E lines in all but one of the sequences.

m depth. Within that stable layer there is a complete reversal of wind direction, from southerly near the surface to almost northerly above that. The altitude of direction reversal coincides with near-zero speeds. Shear is strong ($\sim$0.03 s^{-1}) from the surface to about 380-m altitude (50 m into the cloud); there is little shear throughout the rest of the cloud layer. The main cloud layer is not well defined by the LWC; zero LWC values are found only at about 50 m ASL and below, but there is a change in the vertical gradient of the LWC at the base of the constant-θ_E layer (Fig. 14). Soundings obtained at different times indicate that the base of the inversion rose by about 20 m and cloud base rose by about 50 m during the 1.7-h period of the flight. The cloud layer warmed by about 1°C during that time. These gradients are not large; the rate of rise of the inversion base is only about 50% greater than the mean value over 72 h, and only about a third of the rate reported for 1 day by Gerber et al. (1989).

Soundings for the other two days are closer to the usual pattern for well-mixed, inversion-capped boundary layers (Figs. 2b,c). While some directional wind shear is still evident below the cloud on 15 September (950915), there is none on the last day. The deep near-surface stable layer is gone by these days. The inversion was about the same strength, and the magnitude of the wind shear across the inversion layer was also comparable. On these two days there were no discernible time trends in the soundings; variabilities were on smaller scales.

The dimensionless coordinate ϕ will be used at times to describe cloud depth, with $\phi = 0$ at cloud base and $\phi = 1$ at cloud top. We use this normalization instead of one based on total boundary layer depth, primarily because on one of the days the boundary layer had a complex structure, and because it permits better comparisons of cloud microphysics properties. Cloud base was at 0.60, 0.53, and 0.65 times the total boundary layer depth for the 3 days.

Drizzle was observed to be falling from cloud base and reaching the sea surface in all three cases. Precipitation rates at cloud base were near 0.01 mm h^{-1}. On the first day, 14 September, the rate increased to 0.02 mm h^{-1} near the sea surface due to the presence of the weak cloud in the stable surface layer. On the other two days there was little change below cloud base. The mass concentration of drizzle increased from near 2×10^{-3} near cloud top to about 8×10^{-3} g m^{-3} at cloud base in all three cases. The uniformity of drizzle characteristics is consistent with having similar cloud depths for the last two days; the cloud on the first day was only two-thirds as deep.

4. Echo patterns

a. Images

Reflectivity (Z) and velocity[2] (V) fields, observed with the radar pointing upward, are shown in Fig. 4 for typical flight segments of each of the three study days. Each of these images was recorded during a level flight segment ($\pm$5 m); the vertical scales are altitude above the sea surface. The images are shown with 1:1 horizontal and vertical scales. As mentioned before, each cloud situation was quite steady in time; this is also borne out by the close similarities observed among the 6–10 images recorded at various times during each flight of approximately 1.5–2 h.

The main features to be noted in these images are the relative uniformity of the upper echo boundary and the cellular structure of the echoes. Most of the high-reflectivity cells extend downward from near the echo tops and become more or less sheared through the lower parts of the images. The occasional appearance of stronger echoes not originating at the top is probably related to the orientation of the sample plane relative to the environmental winds. There are no breaks in the echoes. These characteristics apply to all three examples here presented and have been found to be also valid for other stratus cases examined.

Figure 5 shows the shapes of the high-reflectivity cells in horizontal sections. These data are also from level flight segments but with the radar beam pointing sideways from the aircraft. Data from two or three different levels are displayed for each case; the lapse of time between data segments was anywhere from a few minutes to half an hour. An attenuation correction has been applied in each image according to the average LWC observed along the flight segment. Except in the images for the two lower altitudes for 14 September (950914) in Fig. 5, the echo cells exhibit rather irregular and

[2] For simplicity, the term ''velocity'' will often be used to refer to the observed Doppler velocity corrected for aircraft motion. This velocity represents reflectivity-weighted particle velocities with respect to the ground. Upward velocity is positive. If the term Doppler velocity is used, for clear differentiation from air velocities, it also will mean velocities corrected for aircraft motion, not the Doppler velocities actually measured.

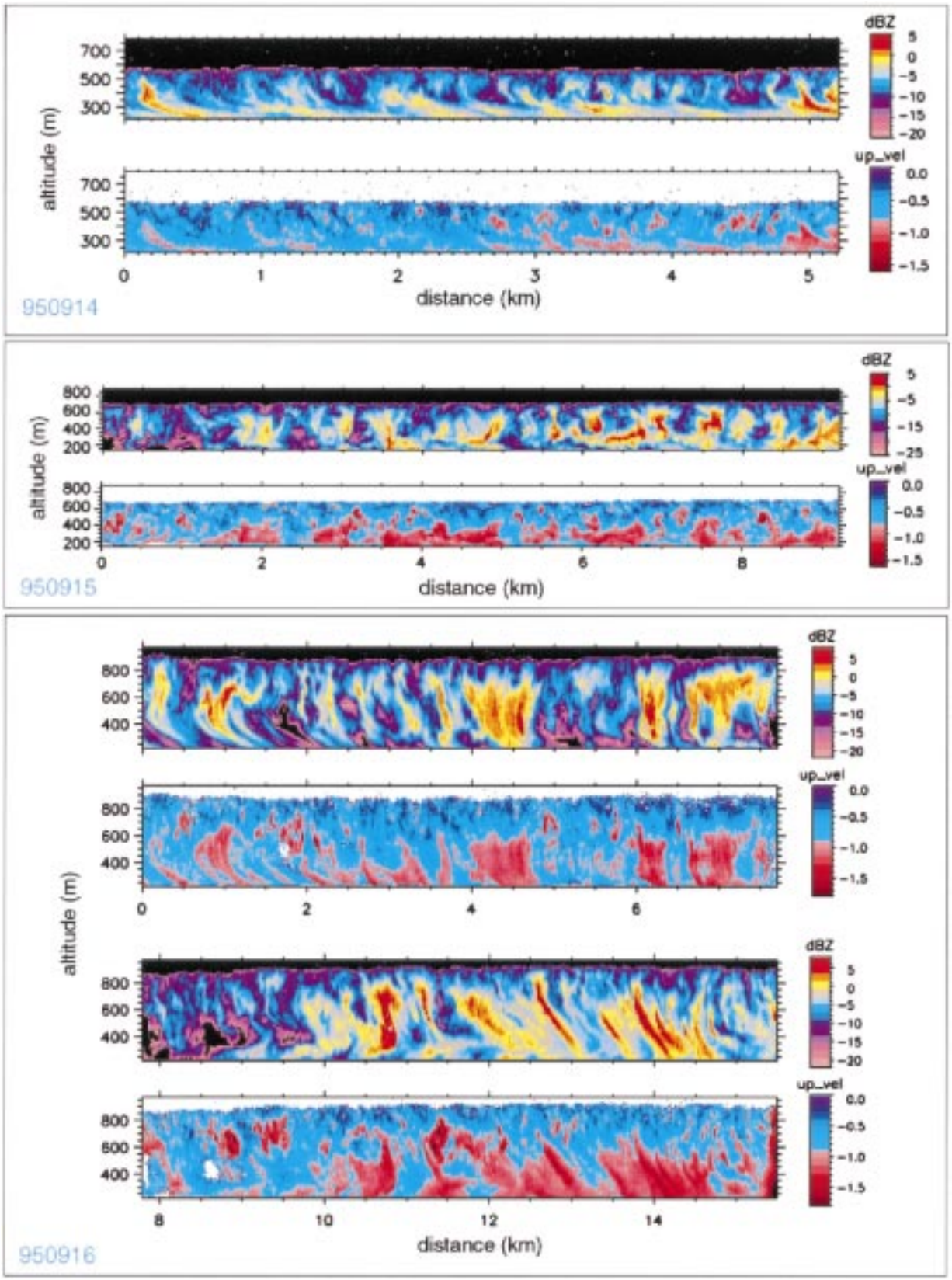

FIG. 4. Examples of vertical cross sections of radar reflectivity (Z) and of Doppler velocity (V, m s^{-1}, positive upward) for the 3 days discussed in the text.

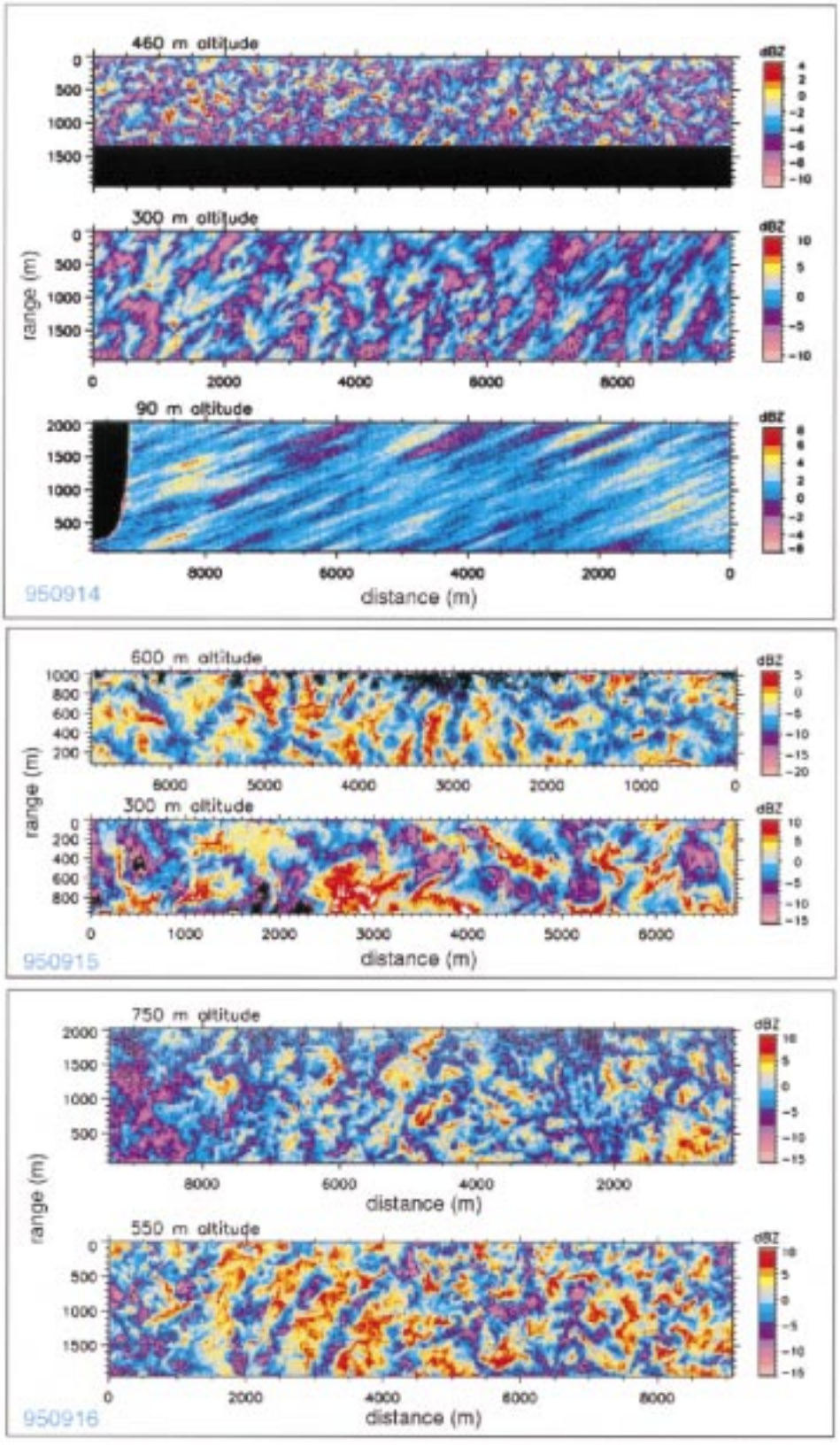

FIG. 5. Horizontal cross sections of radar reflectivity (Z) obtained with the radar in the side-looking position. Altitudes are indicated above each image. Orientation with respect to north is preserved for images from different altitudes for given days.

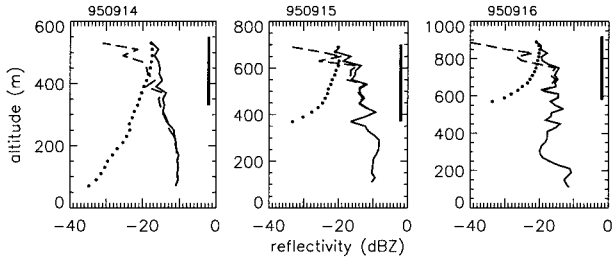

FIG. 6. Contributions to total reflectivity by two size ranges of hydrometeors. Reflectivity $(Z_{calc})_{fssp}$, calculated from the drop size distributions measured by the FSSP probe (<45 μm diameter), is shown by a dotted line and $(Z_{calc})_{twodc}$, from the 2D-C probe (>50 μm), by a dashed line. These data combine measurements made during several ascents and descents through each cloud.

highly intricate shapes. Cell sizes cover quite a large range.

For 14 September, distinct echo streaks are seen to run at a 335°–155° orientation in Fig. 5 for 90-m altitude. There is also some evidence for echo lines of 320°–140° orientation at 300 m. No preferred orientation of echoes is perceptible in the 460 m ($\phi = 0.59$) image. The streaks result from the strong wind shear below 400 m; this is also seen in the vertical sections.

b. Source of reflectivity patterns

Interpretation of the reflectivity and velocity distributions shown in Figs. 4 and 5 must take into account the fact that the relative contributions of different drop size ranges to the reflectivities and to the reflectivity-weighted fall velocities vary with altitude. This drop-size weighting of reflectivity and velocity can be calculated with the help of the size distributions recorded by the in situ probes.

Figure 6 shows the results of this analysis for reflectivity, using data from the ascent and descent soundings. The dominant contribution in the lower parts of the clouds comes from $(Z_{calc})_{twodc}$, the reflectivity due to drizzle drops (>50 μm diameter, from the 2D-C probe), whereas $(Z_{calc})_{fssp}$, the reflectivity due to cloud droplets (<45 μm diameter, from the FSSP probe), becomes stronger near cloud tops. The crossover from drizzle domination to cloud droplet domination occurs at 430 m ($\phi = 0.45$) for 14 September (950914), at 630 m, ($\phi = 0.82$) for 15 September, and at 780 m ($\phi = 0.59$) for 16 September. From this we can generalize that the crossover occurs in the upper two-thirds of the clouds. One evident reason for the crossover to greater contributions to reflectivity by cloud droplets is the increase in LWC and in mean droplet size with height within the cloud.

However, it is important to look beyond average reflectivities in order to establish the roles of different drop sizes in producing the observed patterns of variation about the means. There is little question about the sources of the patterns in the lower portions of the clouds where the absolute values are dominated by drizzle. In these regions it is also found that the standard deviation of $(Z_{calc})_{fssp}$ over contiguous level flight segments of 5–12 km length is typically an order of magnitude smaller than the standard deviation of $(Z_{calc})_{twodc}$ so that the variation in Z is dominated by variations in drizzle drop populations. Furthermore, although essentially no correlation can be found between Z_{obs}, the observed reflectivity, and $(Z_{calc})_{fssp}$, that is due to cloud droplets, positive correlations of 0.3–0.6 are found between Z_{obs} and $(Z_{calc})_{twodc}$. Although this correlation is not as high as it should be, due to the separation between sample volumes and the inadequate sampling rate of the 2D-C probe, the correlation supports the conclusion that drizzle dominates the reflectivity patterns.

Near cloud top, above the crossover to domination by smaller drops, the sample rates for larger drops is so low that it becomes more difficult to extract valid data. This problem is exacerbated by the fact that no long horizontal flights legs were made in those regions. A number of points can nonetheless be made. First, the maximum relative contribution to reflectivity is from droplets of around 30 μm diameter. Second, the standard deviation of the detrended values of $(Z_{calc})_{fssp}$ (10-m resolution data) is only about 1 dBZ, which is considerably less than the variability of the observed reflectivities. Third, in all three clouds, about 10% of the values of $(Z_{calc})_{twodc}$ from regions above the crossover points exceed the highest values of $(Z_{calc})_{fssp}$ for the same regions. Fourth, although much less pronounced toward cloud top, the reflectivity patterns extend without noticeable changes above the crossover heights. These observations suggest that one can extend the conclusion that the major source of variation in reflectivity is the nonuniform spatial distribution of drops >50 μm, and definitely >30 μm, diameter, even to regions near cloud top. As mentioned before, in the lower parts of the clouds drops >100 μm account for the reflectivity patterns.

Since the size dependence of terminal fall velocity further increases the sensitivity of V_{calc} to larger drops, the reflectivity-weighted fall velocity, V_{calc}, is dominated by drizzle drops at all heights except within the last few meters below cloud top where maximum drop sizes are <50 μm.

5. Echo statistics and *Z–V* correlations

Echo intensities at any given altitude in the clouds have a relatively wide range. Statistics[3] of the observed reflectivities and vertical velocities are shown in Fig. 7 for the data segments of Fig. 4. The distribution of dBZ values at a given altitude is quite symmetrical and can

[3] Reflectivity statistics were calculated in terms of Z, then converted back to dBZ.

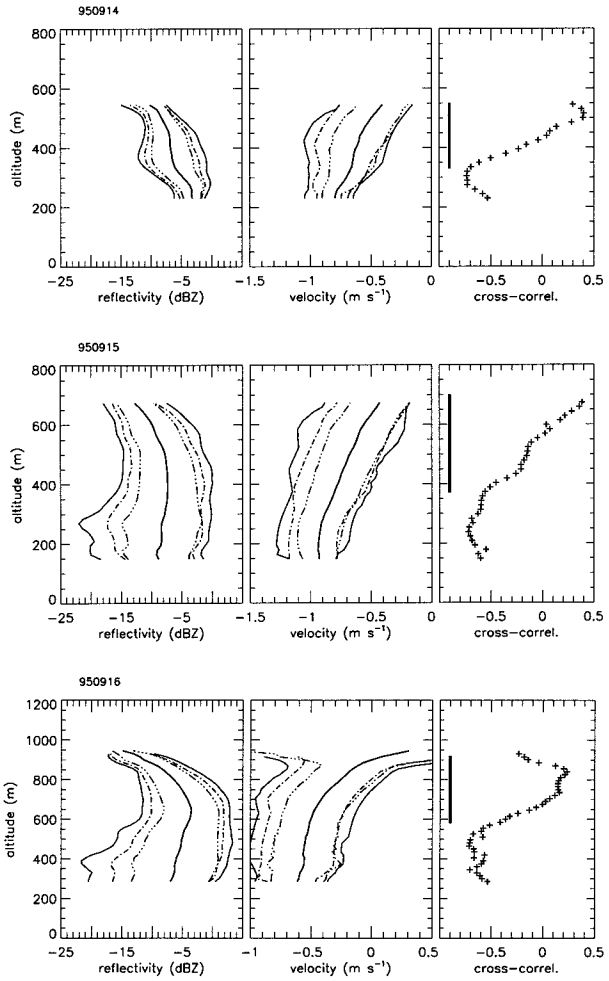

FIG. 7. Vertical profiles of radar reflectivity (Z), Doppler velocity (V, positive-up), and the Z–V correlation coefficient, for the uplooking radar data shown in Fig. 4. In the Z and V profiles, the heavy solid lines show the mean values and the other lines show $\pm$ one standard deviation from the means (triple dots), the 50% ranges (dotted), and the 90% ranges (thin): (a) 14 September 1995 (950914), (b) 15 September 1995, and (c) 16 September 1995.

be well approximated by a normal distribution (log-normal in terms of Z). The average value of the widths of the distributions is around 5 dBZ; this corresponds to a geometric standard deviation of 0.5 for the distribution of Z. It is worth noting the similarity of this value to the geometric standard deviation of 0.39 reported by Cahalan et al. (1994) for LWPs determined by radiometric observations.

Although not in all cases, in general, the spread in reflectivity values is greatest in the drizzle below cloud base where the 95% range covers 15–20 dBZ (factors of 30–100 in Z). In the upper reaches of the clouds this range is about 5–10 dBZ (factors of 3–10 in Z). This latter variation can be accounted for either by variations of about factors of 1.2–1.5 in the diameters, or by factors of 3–10 in the concentrations of drops.

For the majority of cloud volumes where reflectivity is dominated by drizzle, it is interesting to convert reflectivity to drizzle rate. Calculating both reflectivity and rainfall rate from the size distributions measured with the FSSP and 2D probes, we find that the relationship $Z = 10 \times R^{1.0}$ (with Z in mm^6 m^{-3}, and R in mm h^{-1}) represents the central tendency of the data quite well for all three days (within factors of about 2 for $R > 0.05$, and within about a factor of 10 for smaller R). Accepting the exponent of unity means that the average 10 dBZ (factor 10 in Z) range of variation of echo intensity translates into a factor 10 variation in precipitation rate, and the more extreme 20-dBZ range corresponds to a factor of 100 in precipitation rate. Clearly, these are significant deviations from horizontally averaged values.

The mean values of the observed vertical velocities are close to the calculated reflectivity-weighted fall velocities for given altitudes. This is consistent with the expected near-zero mean vertical air velocities. For the first two days (Figs. 7a and 7b), all the observed velocities are downward (negative); that is, no net upward motion of particles is detected anywhere. On 16 September (Fig. 7c), a small fraction of positive values are found near the middle of the cloud and the fraction increases from there upward. However, even in this case one must bear in mind that the magnitudes of the observed positive values are smaller than the estimated accuracies of the vertical air velocity, and hence also of the Doppler velocity, measurements. The general trend to smaller negative (and perhaps some positive) values in the upper regions of the clouds is due to the smaller drop sizes and fall velocities prevailing there. Interestingly, the range of variation of the measured velocities at given altitudes is relatively small, 0.5–0.7 m s^{-1} for 95% of the points. This variation reflects the combined effects of air velocities and of variations in drizzle concentrations and sizes. At least in the upper parts of the clouds, as will be shown later, these two factors work in opposite directions, thus reducing the overall variability.

Even simple visual comparisons of the reflectivity and particle velocity images indicate a considerable degree of correspondence between the two fields. A quantitative expression of this correlation is shown in the rightmost panels of Fig. 7. The main feature of these reflectivity–velocity correlations is a reverse-S pattern; the same pattern is evident in all of the more than 20 instances examined. At low altitudes, higher reflectivities correspond to greater downward particle velocities. This is as would be expected for clouds from which drizzle is falling: higher reflectivity regions indicate larger and faster falling drops. However, in the upper regions of the cloud this pattern reverses: zones of higher reflectivity have *smaller* downward particle velocities. The crossover from negative to positive correlations takes place near $\phi = 0.54$, 0.56, and 0.35 for the three examples shown. Maximum positive correlations are found at $\phi = 0.82$, 0.90, and 0.72 for the three cases.

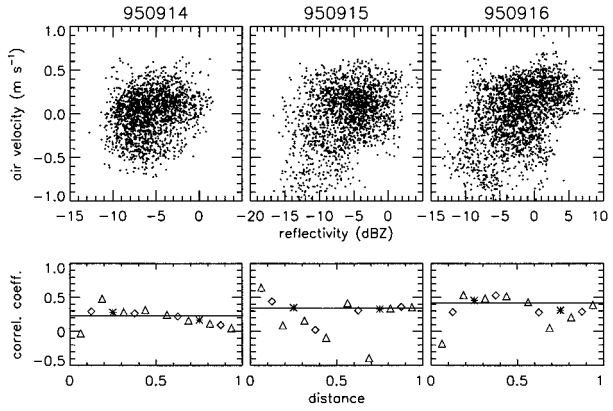

FIG. 8. Vertical air velocity from the in situ probes versus the radar reflectivity 60 m to the side of the aircraft for the data shown in the higher altitude images of Fig. 5. The upper panels show individual data points, each point representing 3.4 m of flight path. In the lower panel, horizontal lines show the correlation coefficients for the entire data segments and different symbols indicate the coefficients over one-half, one-fourth, and one-eighth of the segments (the symbols are placed at the midpoints of the intervals).

Both the crossover point and the position of the maximum have nearly equal values for the first two days and are lower for the third day. It should be noted that the regions of positive *Z–V* correlations start at considerably lower altitudes than where the changeover occurs (cf. Fig. 6) from reflectivities dominated by drizzle drops to reflectivities dominated by cloud droplets. This fact, and the absence of positive (upward) *V* values, rule out the explanation that the positive *Z–V* correlations arise due to the association of ''updrafts'' with higher LWCs.

The reverse-S patterns in *Z–V* correlations appear to be a robust characteristic of the clouds studied, so it is important to examine their origins. Different factors influencing the pattern are explored in the following paragraphs: (i) vertical air velocity versus observed reflectivities, (ii) vertical air velocity versus calculated reflectivities for drizzle, and (iii) diluted downward plumes. These examinations lead to the conclusion that the dominant factor in producing the reverse-S patterns is the vertical transport of drizzle drops.

a. Vertical air velocity versus observed reflectivity

One suggestion for the vertical transport of hydrometeors emerges from the relations between the observed reflectivities Z_{obs} and the aircraft-measured vertical air velocities *w*. Scattergrams of air velocity[4] (*w*) versus reflectivity (Z_{obs}) from the side-looking cases in Fig. 5 are shown in the upper panels of Fig. 8 with each point representing 3.4 m of flight path. These samples are from the middle to upper parts of the clouds (460, 600, and 750 m, or $\phi = 0.59$, 0.70, and 0.50 for the three cases). Weak positive correlations are evident: $r_{wZ} = 0.23$–0.42 (see Table 2). The lower panels in Fig. 8 indicate the correlation coefficients for the entire sample of each case and for subdivisions of it; the latter serve to illustrate the relative homogeneity of the datasets—that is, that not some specific larger-scale cloud region yields the points that dominate the correlation. In contrast with the foregoing, no correlations are found lower down in the clouds, and strong negative correlations prevail in the subcloud precipitation. These data are further characterized in Table 2 with the quantity Δ (dBZ), the difference in average reflectivity for points with air velocities that differ from the mean by at least one standard deviation to either side of it. This quantity indicates that upward air motions are associated with reflectivities that exceed those associated with downward air motions by factors of up to about 2.

b. Vertical air velocity versus calculated reflectivity

Further insight into the relationship between vertical air motion and reflectivity can be obtained by separating the total calculated reflectivities into those due to cloud droplets and drizzle drops. As was already pointed out, $(Z_{calc})_{twodc}$, the calculated reflectivity for drops >50 μm (from the 2D-C probe) is positively correlated with Z_{obs}, (rightmost column of Table 2), but there is no correlation between $(Z_{calc})_{fssp}$ and Z_{obs}. Similarly, there is no correlation ($r < 0.1$) between the measured air velocity, *w*, and $(Z_{calc})_{fssp}$ (using 10-Hz FSSP data). However, significant correlations are found between *w* and $(Z_{calc})_{twodc}$ as shown in Fig. 9. The individual points in this graph represent between 30 and 70 pairs of values, each value being an average over roughly 90 m horizontal distance in the cloud. Except for the points from level flight segments (filled circles), data from three to five separate cloud regions are combined at all levels; in spite of that,

[4] The recorded air velocity values have been adjusted to a zero mean over each flight segment. The offsets were 0.15, 0.3, and 0.13 m s^{-1} for the three cases here considered; these values are within the accuracy of the measuring system.

TABLE 2. Measured reflectivity (Z_{obs}) vs air velocity (*w*).

Date	Altitude (m)	Norm. depth ϕ	Length (km)	$w-Z_{obs}$ correlation r_{wZ}	Δ(dBZ)	$Z_{obs}-(Z_{calc})_{twodc}$ correlation r_{ZZ}
14 Sep 1995	460	0.59	6.8	0.23	1.3	0.30
15 Sep 1995	600	0.70	6.8	0.34	2.3	0.42
16 Sep 1995	750	0.50	8.5	0.42	3.6	0.57

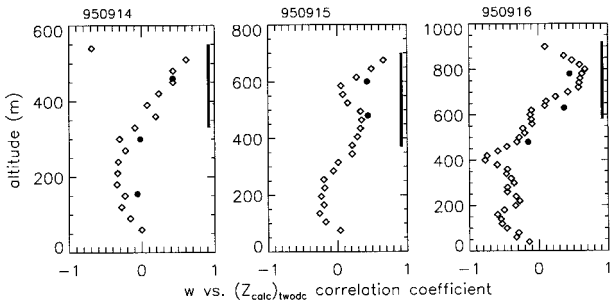

FIG. 9. Correlation coefficients between the aircraft-measured vertical wind (w) and the radar reflectivity $(Z_{calc})_{twodc}$ calculated from drop size distributions measured by the 2D-C probe as functions of altitude. Values indicated by diamonds are based on 1-Hz data from the ascent and descent soundings with roughly 70, 40, and 30 points per height interval for the 3 days. Additional data from continuous level flight segments of 4–6-km length (50–70 s of data) are indicated by circles. Thick vertical lines indicate the altitude of the cloud layer for each case.

the degree of coherence in the data can be said to be quite good. Perhaps more remarkable is the fact that the w versus $(Z_{calc})_{twodc}$ correlation shows the same sign reversal with altitude as was seen for V versus Z_{obs} in Fig. 7. Negative values prevail below cloud base and positive values dominate through most of the cloud depth. Examinations of Z_{calc} versus w scatterplots reveal that, similarly to Fig. 8, the correlation coefficients are not dominated by a small number of extreme values.

The two sets of analyses just discussed, w versus Z_{obs} and w versus $(Z_{calc})_{twodc}$, indicate that upward transport of drizzle drops is one source of the positive correlation between reflectivity and velocity in the upper reaches of the clouds. However, an additional contribution to that relation derives from the downward motion of parcels diluted by entrainment mixing.

c. Diluted downward plumes

One indication for downward-moving parcels with stronger than average velocities is seen in the few points with large negative air velocities and weak reflectivities in Fig. 8; in terms of V the downward velocities would be even stronger. Yet further evidence for the downward motion of diluted parcels is shown in Fig. 10 where narrow reflectivity and velocity ranges are highlighted for the images of Fig 4. The highlighted reflectivities are relatively low values, and they are surrounded by higher reflectivities. The highlighted velocities are nearly the largest negative values for the entire field, and these regions are surrounded by smaller negative velocities. Many of the highlighted reflectivity zones extend downward from cloud top and suggest downward-penetrating plumes. In most cases this is confirmed by the velocity pattern. There are particularly striking examples of the these plumes at the horizontal locations 2700, 3400, and 4500 m in Fig. 10a. In these instances the plumes start at cloud top, extend downward more than 200 m, and terminate less than 100 m above cloud base. The general prevalence of high-velocity regions in the lower parts of the images is, of course, due to the larger fall velocities acquired by the growing drops.

Detection of the downward incursions in the hydrometeor data from the in situ probes is made elusive by the small, 50–100 m, sizes of the regions. Only 5–10 data points are registered by the FSSP probe over that distance, and the 2D imaging probe has no useful resolution on that scale for the low drizzle drop concentrations prevailing in these clouds. As mentioned before, at lower levels in the clouds no correlations exist between the reflectivity due to cloud droplets and the vertical air velocity; the diluted plumes represent too small a fraction of the total volume, and conditions in them deviate from the means so slightly, that their effect is not discernible in terms of correlations. Some relatively clear examples of the phenomenon have been found near the tops of the clouds. Figure 11 shows two such examples from slow traverses of the cloud tops. In the first example (Fig. 11a), a region of low reflectivities is seen between 300- and 400-m horizontal distance; corresponding low vertical air velocities are seen in the upper panel. This feature occurred only about 10 m below the altitude where the aircraft emerged from the cloud at 750-m horizontal distance. The second example (Fig. 11b) covers a larger horizontal region from a descent into cloud at an approximate rate of 50-m altitude loss per kilometer of horizontal travel. A number of interesting points are shown by these data. The temperature minimum occurs well into the cloud, about 50 m below the altitude of cloud entry. Sharp decreases in velocity, with accompanying decreases in LWC and in reflectivity are seen at 0.9 km, and in three interrupted segments between 2.8 and 3 km. The latter segment is 130 m below cloud top. These are patterns expected for diluted mixtures. It may also be noted that the incursion at 0.9 km is associated with a rise in temperature, whereas the incursions at 2.8–3 km are associated with decreases in temperature; this results from the fact that the aircraft is descending through the inversion, so that temperature is increasing with time (decreasing altitude) at 0.9 km while the gradient is the opposite at 2.8–3 km.

d. Upward transport of drizzle

The conclusion that can be drawn from the empirical evidence in Fig. 7 and from the foregoing analyses (remembering that all observed values of V are negative) is that the positive correlation between Z and V in the upper parts of the clouds is due to a combination of two causes: upward transport of drizzle drops and the downward motion of regions diluted by entrainment. We are unable to make a rigorous separation between the contributions made by these two processes. However, positive correlations of both the observed and calculated reflectivities with vertical air velocity, the substantial

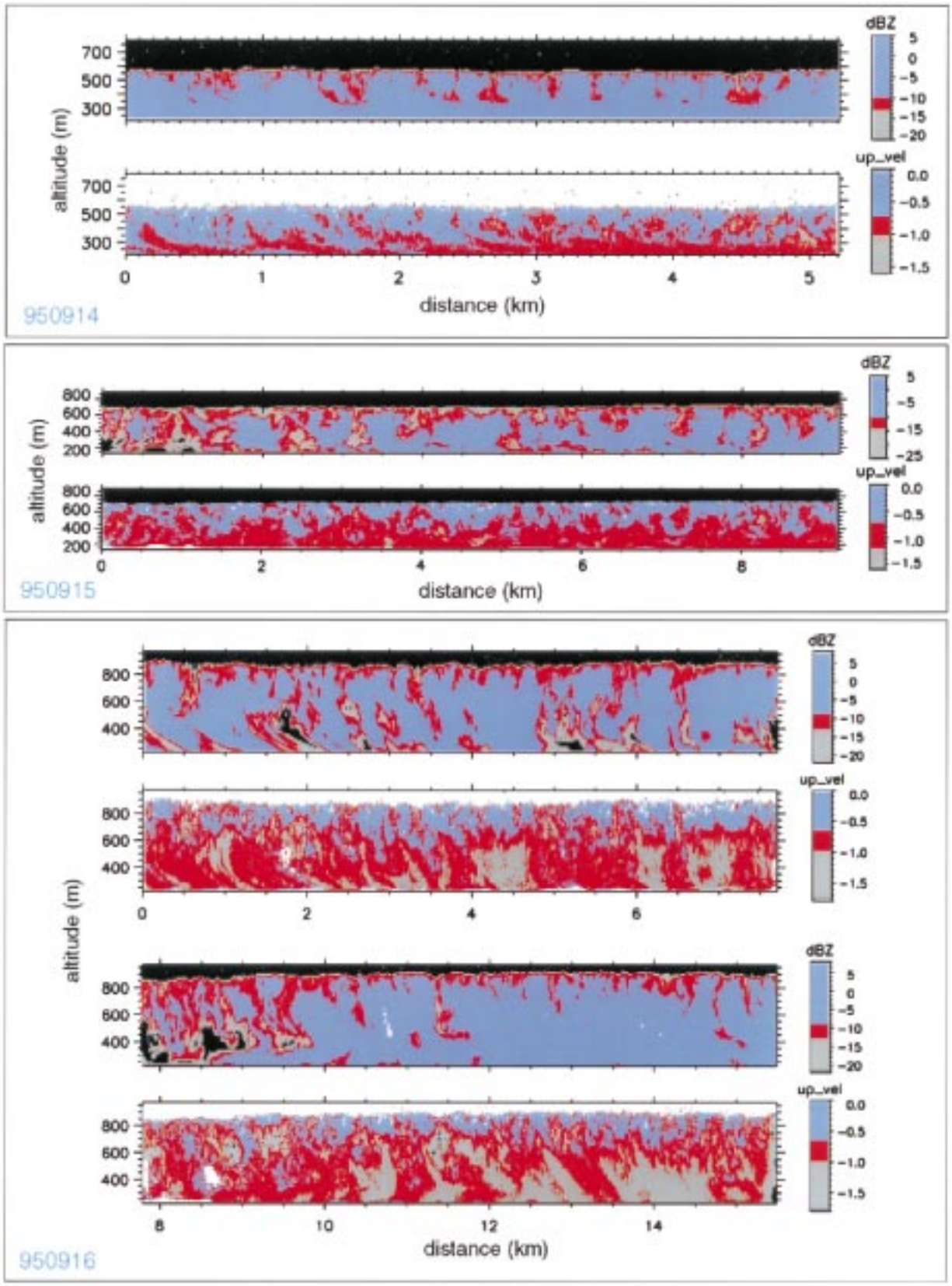

FIG. 10. The same vertical cross sections of radar reflectivity (Z) and Doppler velocity (V) as those shown in Fig. 4 but with Z and V contour levels changed to highlight areas having relatively low reflectivities and large negative (downward) velocities.

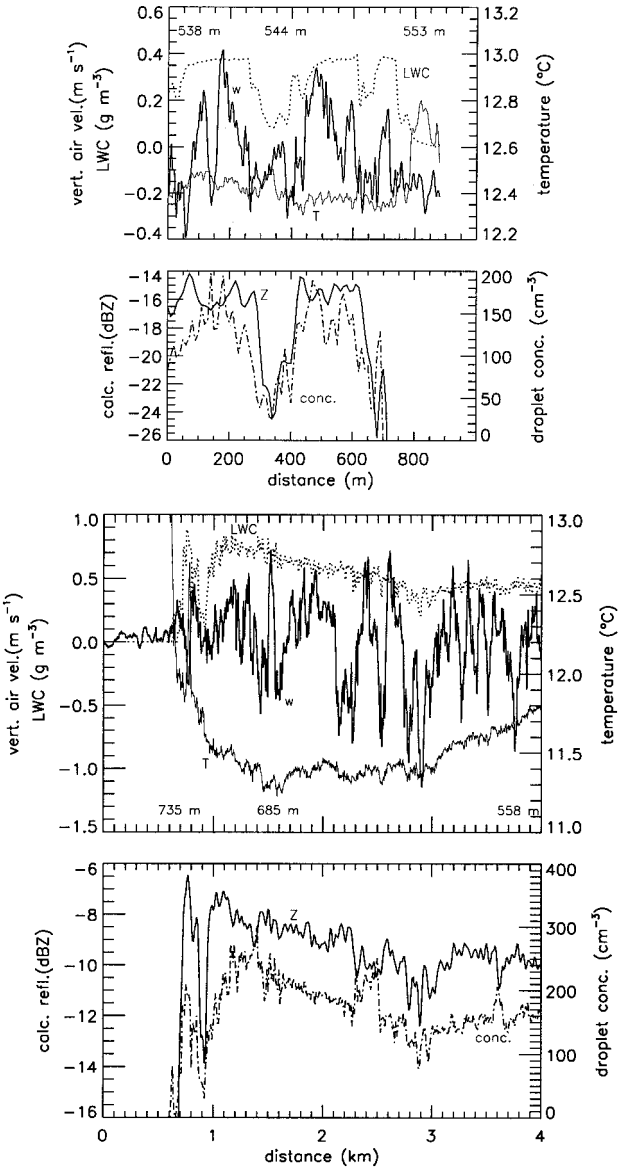

FIG. 11. (a, upper panels). Traces of aircraft-measured vertical winds (w), temperature (T), LWC, droplet concentration, and calculated reflectivity for an ascent through cloud top on 14 September 1995. The numbers above the top panel are aircraft altitudes. The LWC was derived from the CSIRO probe. Droplet concentration and reflectivity are based on FSSP data. (b, lower panels). Same as (a) except for a gradual descent into cloud on 15 September 1995. The LWC content in this figure is based on FSSP data. Aircraft altitudes are indicated at the bottom of the top panel.

difference in reflectivities associated with upward and downward air motions, and the absence of correlations between w and $(Z_{\text{calc}})_{\text{fssp}}$ all indicate that the upward transport of drizzle drops is likely to be the stronger contributor.

Thus far the upward transport of drizzle drops was characterized in terms of reflectivity. Clearly, the transport should also be evident in terms of number concentration and in terms of mass of the drizzle drops as well. To demonstrate that indeed this is the case, the correlation between vertical air velocity and the mass concentration of drizzle drops, $\text{LWC}_{\text{twodc}}$, is shown in Fig. 12 for one of the study days. This plot can be compared with the rightmost panel in Fig. 9. Just as in terms of reflectivity, negative correlations dominate below cloud base and positive ones in most of the cloud layer. The largest positive values are found just above the middle of the cloud. The decreased correlations near cloud top are due, at least in part, to the poor sampling of drizzle drops in that region by the in situ probes. More will be said about these correlations in section 8.

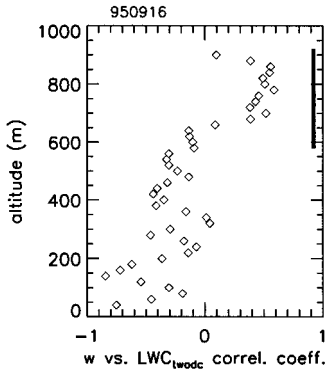

FIG. 12. Correlation coefficients for vertical air velocity vs mass of drizzle drops (>50 μm diameter) at different altitudes based on data collected with 90-m resolution during a series of ascents and descents through the cloud layer on 16 September 1995. The depth of the cloud layer is indicated by a heavy vertical line.

The radar data indicate that upward transport of drizzle drops is present on scales at least as small as about 4–5 m, whereas the in situ data show a similar pattern on scales of around 90 m. Our in situ measurements of drizzle drop concentrations do not have sufficient resolution to examine fluxes on scales comparable with the radar data. It is also beyond the scope of this study to comment on the spectral distribution of turbulent transport or the magnitudes of the fluxes.

6. Liquid water content

As shown in the soundings of Fig. 2, the LWC[5] profiles on all three days exhibit the usual triangular profile. There are, however, significant differences to be noted. In Fig. 13 the LWC measurements are presented in greater detail and the observed values are compared with those expected for a saturated parcel lifted adiabatically from cloud base. In each case, data are combined from three to five ascents and descents through the cloud layer. Mean, and 50th and 90th percentile values of

[5] The contribution of drizzle to the LWC is always small so that the LWC essentially reflects the mass of cloud droplets <50-μm diameter).

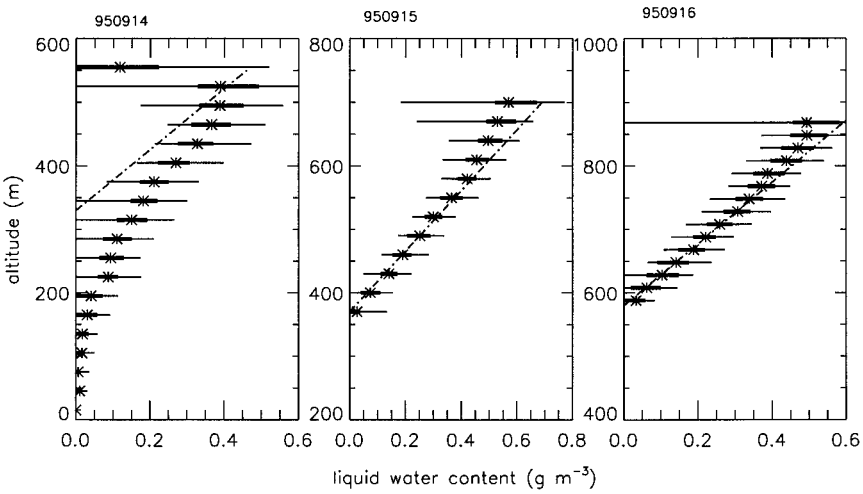

FIG. 13. Profiles of LWC calculated from drop size distributions measured by the FSSP probe. Data for each day are combined from several soundings. Mean values are indicated by asterisks, the thick bars encompass the 50th percentiles, and the thin bars show the range of values to the 90th percentiles. Broken lines show LWC values that would occur for adiabatic ascents of saturated parcels.

LWC are shown. All values are averaged over the time spent by the aircraft in the given altitude intervals so that zeros are also included. Except for altitudes above 540 m, 650 m, and 860 m (the last two points on each profile) and below cloud base for 14 September 1995 (330 m), the fraction of flight time with nonzero LWC values exceeded 95%. This confirms the visual continuity of the clouds and indicates that the observed decreases in LWC with respect to adiabatic values near cloud top did not result from averaging over cloudy and clear zones. The total lengths of the flight segments represented by data points in each height interval are about 3–6 km.

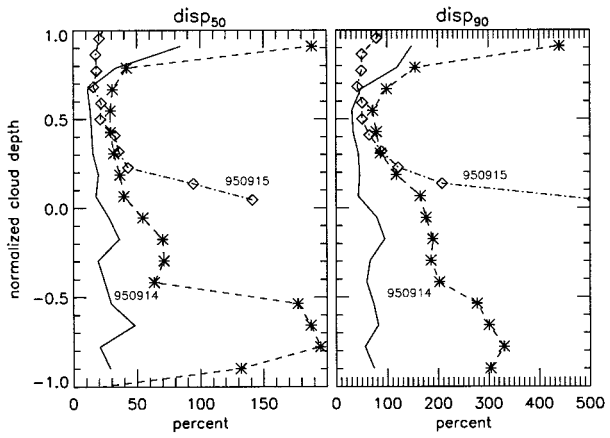

FIG. 14. Profiles of ''dispersion'' values for LWC for 14 and 15 September 1995, plotted as functions of normalized cloud depth (ϕ). The first panel shows dispersions calculated as the 50th percentile range of LWC values divided by the means at each level; the second panel uses the 90th percentiles. Each panel contains data from the FSSP (asterisks for 14 September; diamonds for 15 September) and the CSIRO probe (solid line for 14 September only).

For 15 September and 16 September the profiles are close to the adiabatic values from cloud base to about two-thirds of the cloud depth. For 14 September the observed profile is almost totally incompatible with the notion of parcel lifting; this case will be examined in more detail in section 10.

The data in Fig. 13 were derived from the FSSP probe and have 10%–30% probable errors. For the flight of 14 September, data are also available from the CSIRO probe; data from this probe show the same profile and have even less variability. However, the LWC values from the CSIRO probe are only about 68% of the values derived from the FSSP, with the relationship $\mathrm{LWC}_{\mathrm{csiro}} = 0.63 \times (\mathrm{LWC}_{\mathrm{fssp}}) + 0.02$. The major mass contribution in these clouds comes from near 30-μm diameter droplets at all altitudes; there are no obvious shortcomings of either instrument for droplets of those sizes, so the source of the difference between the two instruments remains unexplained. This uncertainty in the LWC measurements indicates that the actual LWC was perhaps not as close to the adiabatic values as is depicted in Fig. 13.

Another aspect of the difference between 14 September and the other days can be seen in the variabilities of the observed LWC values. Vertical profiles of the variances of the LWC measurements are shown in Fig. 14 expressed as fractions of the means for given heights and using the normalized cloud depth parameter ϕ. Although not shown, the dispersion profiles for 16 September are identical to those of 15 September. The sharp increase in dispersion for $\phi > 0.6$ on 14 September is in remarkable contrast with the nearly constant values observed on the other days. The CSIRO probe data yield even lower dispersion values than the FSSP data (in spite of using 30-Hz CSIRO data versus 10-Hz FSSP

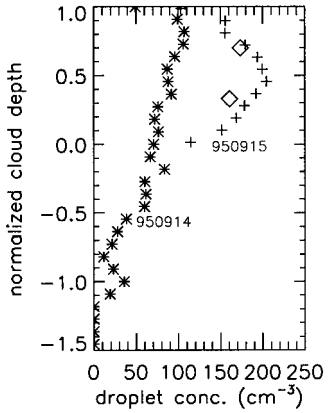

FIG. 15. Profiles of droplet concentrations for 14 September 1995 (asterisks) and for 15 September 1995 ("+"), plotted as functions of normalized cloud depth (ϕ). The diamonds show average concentrations from horizontal aircraft passes on 15 September.

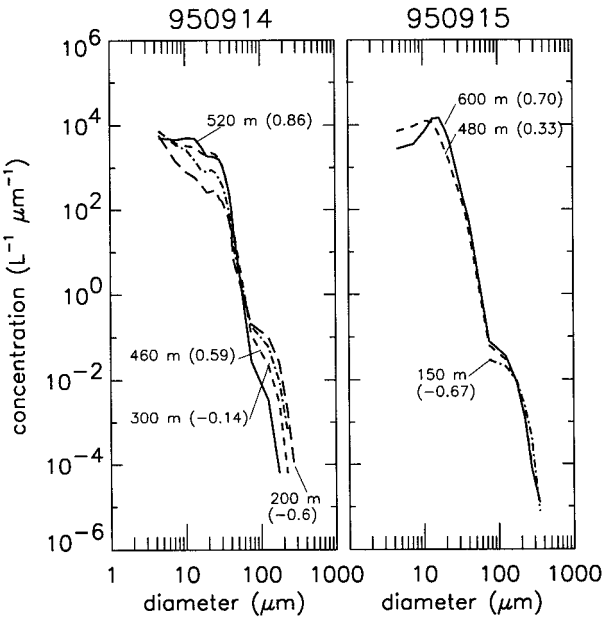

FIG. 16. Average drop size distributions (FSSP and 2D-C data) for horizontal passes at different levels on 14 and 15 September 1995. The labels indicate the geometric height above sea surface (m MSL) and the corresponding normalized cloud depth level (ϕ).

data) further underscoring the uniformity of the LWC for given altitudes.

In contrast with the uniformity of LWC, the number concentrations of cloud droplets exhibit great variability, with dispersion values up to and exceeding 100%. This variability is offset, however, by a strong negative correlation ($r \approx -0.7$) between number concentration and mean droplet size. This fact was also noted by Hudson and Li (1995).

7. Size distribution

The concentrations of cloud droplets exhibit different vertical profiles for the different days. These data are shown in Fig. 15 for 14 September and 15 September. As for the LWC plots, the indicated values are averages over the entire duration of flight in each height interval, including zeros where they occur (only at $\phi = 0.9$ and 1.0, and at $\phi < 0$). Maximum concentrations were 100–120 cm^{-3} on the first and third days, whereas the day in the middle had concentrations reaching 200 cm^{-3}. Highest concentrations occurred at $\phi \approx 0.8$ on 14 September and at $\phi \approx 0.5$ on the other two days; as will be seen, this is due to the differences at the small ends of the size spectra.

Size spectra, averaged over level flight segments are shown in Fig. 16 for the first two days. Data from the FSSP and 2D-C probes are combined in these diagrams. The breaks near the middle of the curves correspond to the change from one probe to the other; it is unresolved to what extent the breaks are real and to what degree they result from undersampling of drops in the smallest size interval used for the 2D-C probe (50–100 μm). The spectra for the two days differ in two important respects. First, although the concentrations of the smallest droplets remain high for all altitudes on 14 September, there are significant decreases from the peak values on 15 September and the decreases become more pronounced with increasing altitude. Diminished concentrations of small droplets with time are expected for condensational and coalescence growth. We do not have an explanation for the source of the smallest droplets found at all heights on 14 September. Second, there are substantial increases in the concentrations of drizzle drops with decreasing altitudes on 14 September; corresponding changes on 15 September are barely perceptible. The growth observed on 14 September is consistent with the presence of cloud droplets below the main cloud base (330 m, $\phi = 0$) leading to continued growth of drizzle drops by coalescence.

Using data from the combined soundings, changes in the average size spectra with altitude can be depicted as in Fig. 17. In both cases the concentrations of drizzle drops increase from the top down. The concentrations of cloud droplets in each size category increase upward consistent with droplet growth. The first three size channels show an exception to this pattern for 15 September. Drizzle drop concentrations in the range 50–150-μm diameter were higher on 14 September by factors of about 2. The two sets of data are nearly identical in the size range 25–45 μm.

Precipitation rates near cloud base, calculated from the in situ probe data, were in the range of 0.05–0.01 mm h^{-1} on both days. Below cloud base the rate increased to 0.015 mm h^{-1} on 14 September.

8. Velocity variances and correlations

The observed variances of vertical velocities reveal some differences among the study days. The variances

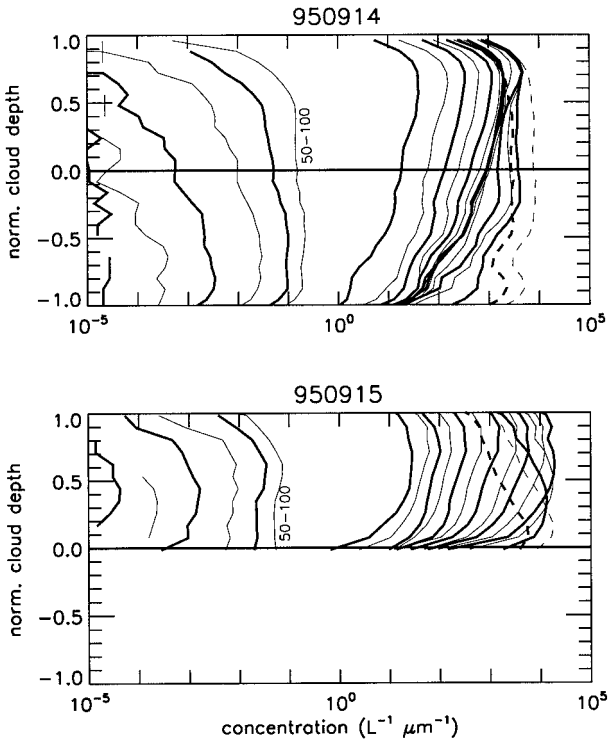

FIG. 17. Drop size distributions as functions of altitude on 14 and 15 September 1995. From right to left, alternating heavy and thin lines indicate the differential concentrations for each of the 15 size bins used for the FSSP data (3–45 μm in 3-μm intervals) and for 5 size bins extracted from the 2D-C data (50–100 μm, 100–150 μm, etc.). In each panel, the dashed lines are for the first and second FSSP size bins.

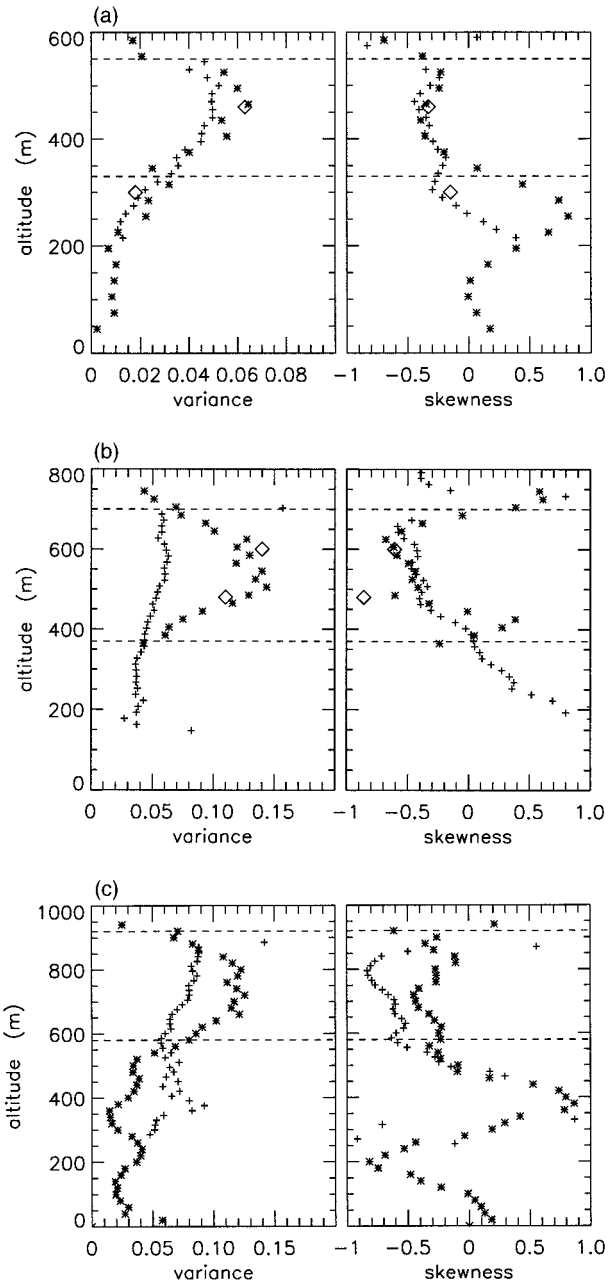

FIG. 18. Profiles of variance and skewness for aircraft-measured vertical winds (w, asterisks and diamonds) and radar Doppler velocities (V, + signs). Diamonds refer to vertical wind data from horizontal aircraft passes, whereas asterisks refer to data from ascents and descent soundings. The Doppler velocities are from a data segment of approximately 5-km length: (a) 14 September 1995, (b) 15 September 1995, and (c) 16 September 1995.

of the Doppler velocities var(V) and of the air velocities var(w) are shown in Figs. 18a–c. Sampling rates for these two quantities are nearly the same (30 and 20 Hz). Peak values of var(V) occur at about two-thirds cloud depth and have comparable values of $\approx$0.05–0.07. Profiles of var(w) have maxima near the middles of the cloud layers on all three days but the values are about only half as large for 14 September than for the other two days. Especially on 15 September and on 16 September, var(w) is considerably greater than var(V). This is not surprising in view of the negative correlation between w and drizzle drop concentration, plus the fact that V is determined by the velocities of the drizzle drops.

The skewness of the air velocity and Doppler velocity distributions (right-hand panels in Fig. 18) have similar vertical variations and have comparable values. This is somewhat surprising in light of the fact that the aircraft data for w are composites for entire flights, whereas the radar measurements of V shown in these figures are relatively short data segments. For all 3 days, negative skewness values prevail within the cloud layers and positive ones below cloud base. Negative values within the cloud are consistent with the likely source of in-cloud turbulence being at cloud top, whereas positive values below cloud base are to be expected to be associated with an upward buoyancy flux.

The variance of the Doppler velocity in the horizontal, var(V_h), was also evaluated for some flight segments at constant altitudes and with the antenna in the side-looking mode. These results are shown in Table 3 along with

TABLE 3. Variances of horizontal and vertical velocities.

Date	Altitude (m)	Norm. cld. depth ϕ	var(w)	var(V)	var(V_h)
14 Sep 1995	460	0.59	0.07	0.05	0.09
	300	−0.14	0.02	0.02	0.08
	160	−0.77	—	0.01	0.03
15 Sep 1995	600	0.70	0.14	0.05	0.07
	480	0.33	0.10	0.05	0.10, 0.14
16 Sep 1995	780	0.59	0.12	0.07	0.15
	630	0.15	0.07	0.06	0.16

values of var(w) and of var(V) for the same altitudes from Fig. 18. In spite of scatter, in part due to the lack of simultaneity in the measurements of the various parameters, it is clear that the var(V_h) > var(V) and that var(V_h) ≈ var(w). The latter near-equality supports the validity of the measurements, because it is consistent with the expectation that V_h and w have similar distributions in nearly isotropic turbulence.

As a summary, and as reinforcement for the connections between air motions and hydrometeor populations already discussed, correlations between the vertical air velocity w and other parameters are indicated in Table 4. Level flight segments without turns have been used for these analyses. The highest resolution available was used for each parameter: 30 Hz for w and for temperature, 10 Hz for FSSP, and 1 Hz for 2D-C data. To match the slower parameters, w was resampled after filtering with an eighth-order nonrecursive low-pass filter with a cutoff frequency of 4 or 0.4 Hz.

The correlations between w and temperature are generally weak, but they do show a systematic sign reversal between in-cloud and below-cloud values. Although we have not attempted to quantify the fluxes, it appears to us that heat fluxes were relatively small in the clouds examined, were opposed by stability below the main cloud on 14 September, and were inhibited even in the unstable layer around 480 m ($\phi = -0.29$) on 16 September.

The relation between vertical velocity and cloud droplet concentration deserves an additional note. Although the scatterplots of most other pairs of parameters appear relatively uniformly spread across the range of values, the droplet concentration versus vertical air velocity plots have characteristic ''golf club'' shapes, as shown in the top panels of Fig. 19 with each point representing about 10 m of horizontal distance through the cloud. As these diagrams indicate, negative air velocities are associated with low droplet concentrations, whereas at positive air velocities the droplet concentrations cover a large range, to maxima well above the mean values. The lower panels in Fig. 19 indicate how these patterns translate into frequency distributions for points with air velocities that differ from the mean by more than one-half standard deviation. There are considerable differences between the pairs of distributions for upward and downward air velocities, specially in the tails toward large concentrations. For each of the three datasets shown in Fig. 19, the lowest altitude has been chosen for which adequate data were available. For 15 September and 16 September, data from higher altitudes were also examined; these show the same patterns but the distributions for positive w do not extend to as high values as at the lower altitudes. These results are consistent with the creation of new cloud droplets at cloud base in upward-moving parcels as has been seen already in the size distributions shown in section 7. The correlation with w confirms the role of upward air motions in the formation of new drops. Closely coupled with these results are strong negative correlations between droplet concentrations and average droplet sizes, leading to relatively modest variations in LWC at any given altitude.

9. Horizontal scales

Scales of horizontal variation of echo intensity and Doppler velocity were examined using Fourier spectral analysis of uplooking radar data during straight, constant-altitude aircraft passes at or below cloud base. Figure 20 presents data from one such pass on each of two

TABLE 4. Correlations with air velocity (w).

	14 Sept 1995			15 Sept 1995		16 Sept 1995		
Altitude (m)	460	300	155	600	480	780	630	480
Norm. cld. depth, ϕ	0.59	−0.14	−0.77	0.7	0.33	0.59	0.15	−0.29
Temperature	0.21	−0.13	−0.21	*		0.32	0.19	−0.10
Drop concentration	0.58	0.30	−0.13	0.39	0.44	0.29	0.44	−**
Mean drop size	−0.53	−0.26	−0.04			−0.23	−0.38	−
LWC_{FSSP}	0.16	0.06	0.07	0.21		0.0	0.0	−
LWC_{CSIRO}	0.30	−0.01	−0.15					
Drizzle conc.	0.44	−0.04	−0.03	0.45		0.42	0.27	−0.11
Drizzle mass	0.50			0.42		0.45		

* Empty boxes indicate data not available or not calculated.
** Dash (—) means that no cloud was present.

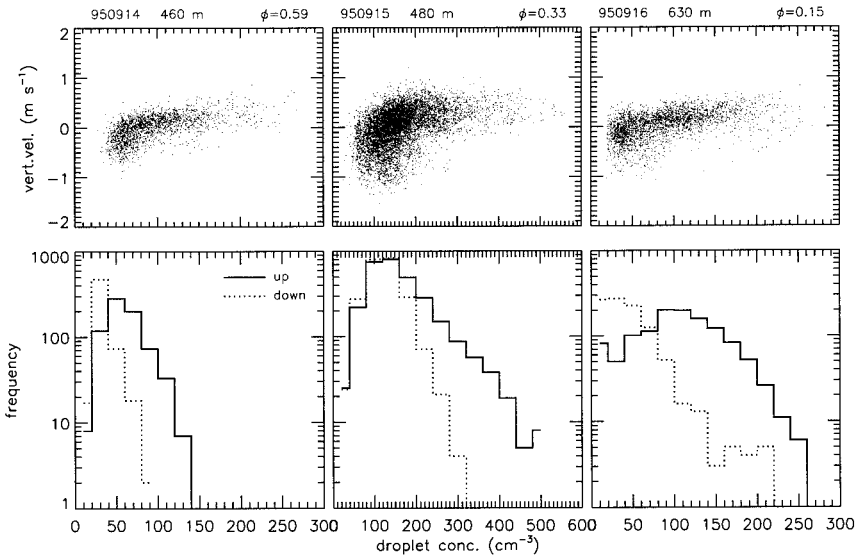

FIG. 19. The relationship between droplet concentration and vertical air velocity during level flight segments within clouds. Each point in the upper panels is a sample from approximately 10 m horizontal distance. The histograms in the lower panels show the droplet concentrations associated with air velocities differing from the means by more than 0.5 standard deviation.

of the study days. Spectral and cospectral densities were calculated for each range gate that had continuous data, then combined as contour plots in Fig. 20. Although originally calculated as functions of frequency, the values are contoured here in the spatial domain of altitude and wavelength (true airspeed/frequency). The base-10 logarithms of spectral density for Z and V are contoured in the first two panels of each figure; negative values correspond to magnitudes less than 1. The Z–V cospectral densities are contoured in the last panel. The cospectra have the same signs as the corresponding correlation coefficients (Fig. 7), with the dominant values being positive in the upper cloud layers and negative in the subcloud layers.

On 14 September, the horizontal scales of variation change with altitude. The Z and V spectra and the Z–V cospectra are strongest at wavelengths of about 1200 m in the upper cloud layer (370–520 m; see also Fig. 2a), and about 1700 m in the layer below that. As shown in Fig. 4, the change in scale probably resulted from the fact that not all of the high reflectivity areas in the upper cloud layer had corresponding high reflectivity areas in the layer below. The most likely cause of this is the strong shear, and the fact that the vertical plane sampled by the radar was not lined up with the wind direction, resulting in spread-out precipitation trails crossing into the sample plane. In contrast, on 16 September there was no directional shear, so that nearly all the high reflectivity areas were continuous from the cloud layer to the sampling level. The resulting spectra and cospectra show the strongest scale of variation to be about 1300 m at all heights (Fig. 20).

These analyses are relatively simple attempts at characterizing the echo structure. Brief looks at parameters other than radar reflectivity, which is principally a reflection of the spatial distribution of drizzle, revealed no structural characteristics, but this aspect needs further examination. The influence of the relative orientation of the flight line with respect to the winds also needs more detailed attention. Furthermore, the horizontal echo maps (Fig. 5) offer opportunities for more detailed analyses than those included here.

10. Discussion

Some comments are in order to round out the information given in section 3 regarding general conditions during the 3 days of the case studies. The coastal stratus cases described here differed from the thermodynamic characteristics frequently associated with marine stratocumulus most importantly in that air immediately above cloud top and to some distance beyond the inversion top was not dry; in fact, mixing ratios changed little across the inversion in our cases. In addition, on the first day, the cloud layer was advecting into the region above a deep stable layer; other than that the boundary layers were well mixed. Wind profiles varied remarkably during the 3 days: near-surface winds veered from southerly to westerly, winds above the inversion veered from NNE to E, and winds in the cloud layers backed from N to NW. Wind shear was always strong across the inversion and was also strong in the subcloud layer on the first day. With respect to radiational forcing, the three days were quite similar, as all three sets of observations were made during the late morning hours and there were no upper-level clouds in any of the cases.

In the following paragraphs, specific topics are taken up to round out the analyses presented in the preceding

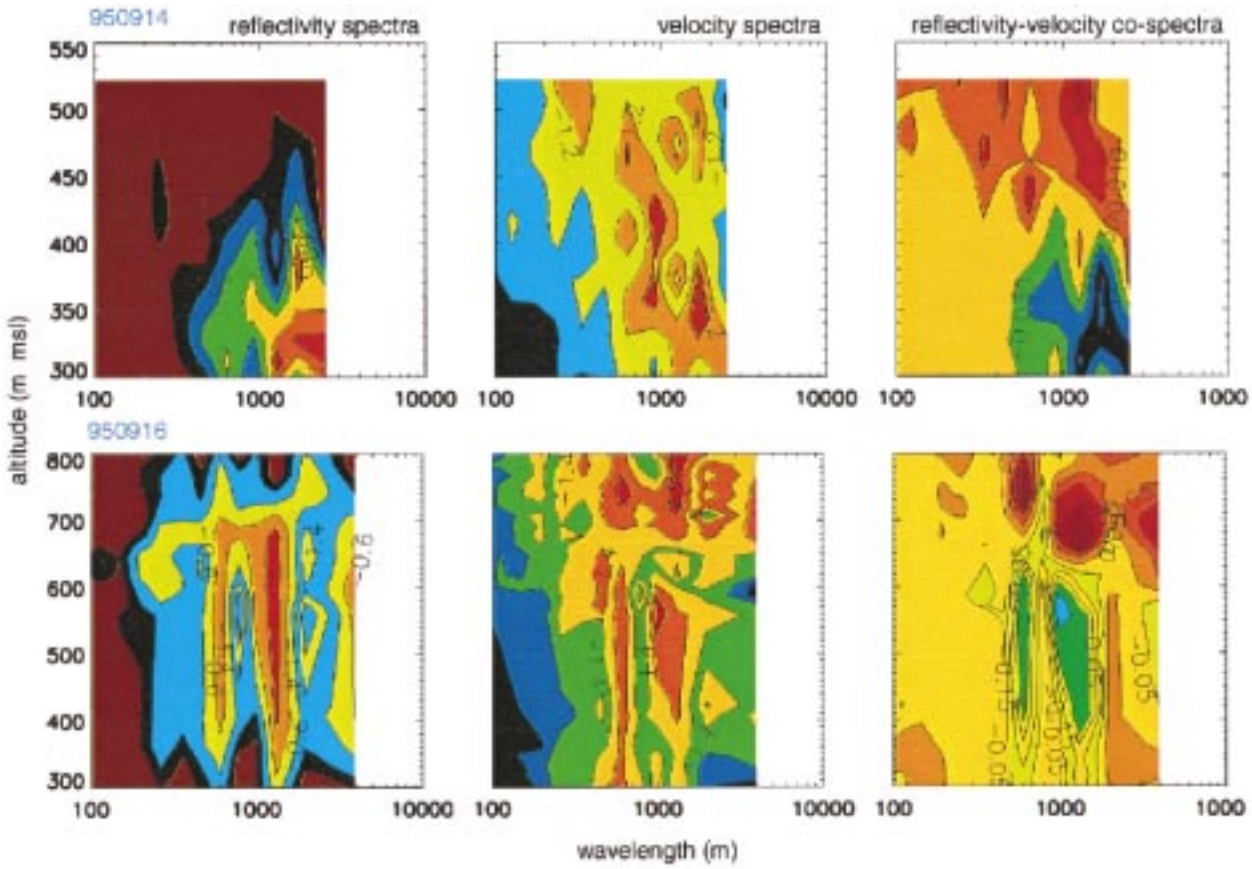

FIG. 20. Spectral and cospectral densities for radar reflectivity (Z) and Doppler velocity (V) as functions of altitude on 14 and 15 September 1995. Data are from 5- to 20-km segments of uplooking radar data. In the first two panels the contour values are base-10 logarithms of spectral density; in the third panel the contour values are actual cospectral densities. The red-to-violet color progression corresponds to a numerical progression from positive to negative.

sections, and to compare the findings with those of other authors.

a. The 14 September (950914) case

The cloud studied on 14 September had the most unusual features, which deserve some additional discussion. First of all, this cloud was cut off from moisture supply at the surface by the stable layer between the ocean surface and 300 m. The air temperature measured at the lowest flight level (65 m) was 12°C on this day, 2°C colder than either the day before or the two subsequent days. Although we have no measurements of sea surface temperature from the flight location, buoy and ship data from within a 100-km region support the assumption that there was a brief incursion or upwelling of cold water in the area on 14 September. Evidently, the cloud above the stable surface layer was advected into the region and was precipitating. About 7 h would be required to deplete the water content of the cloud at the observed precipitation rate. Traveling with a speed of 6 m s^{-1}, the cloud would move 150 km over that period. That is about four times the extent of the study area. Temperature within the cloud at any level had a N–S gradient of about 0.5°C per 10 km, which translates (at 6 m s^{-1} wind speed) to a cooling of -1.1°C h^{-1}. However, this cooling was offset by the warming of $+1.1$°C h^{-1} that was evident in the temperature measurements when returning to given locations over the study period. The net effect on a parcel of cloudy air advected toward the south would be roughly no temperature change. The accuracy of these heating and cooling rates is relatively poor, since they are obtained from data collected during a complex flight pattern. In fact, the apparent steady state of the cloud is readily explained by an overall cooling, by radiation and by mixing with cold air near the sea surface, of only about 0.1°C h^{-1}. That much cooling is sufficient to offset depletion by precipitation.

Other surprising features of the 14 September case were the presence of cloud within the low stable layer and the monotonic LWC profile from the surface to the top of the main cloud. Cooling from the sea surface was no doubt producing the positive temperature gradient within the stable layer and was deepening it, whereas at the same time the main cloud layer was getting ''erod-

ed'' from the base up. The Richardson number within the stable layer is about 0.9, indicating the possibility of dynamic instability and enhanced vertical mixing. Thus, the observed structure is probably a combined result of cooling within the stable layer, maintaining saturated conditions there in the manner of an advection fog, and of mixing with the main cloud layer above it.

Although the wind shear within the stable layer extended into the lower few tens of meters of the main cloud on 14 September, the turbulence generated by this within the main cloud layer was less intense than that generated by buoyancy forces on the other two study days. Evidence for this is seen in the roughly factor 2 lower values of var(w) on 14 September than on the other days (cf. Fig. 18).

The correlations (cf. Tables 2 and 4) between w and temperature and hydrometeor parameters are not significantly different for this day from values obtained for the other days.

b. Drizzle

One general characteristic of the coastal stratus we studied was the prevalence of drizzle. Drizzle drops, in concentrations corresponding to precipitation rates up to 0.2 mm h^{-1}, were found in 10 of the 12 clouds sampled on that many different days. The cases with drizzle included a large range in droplet concentrations (160–800 cm^{-3}) with no clear correlation to drizzle rate. Cloud depths varied between 150 and 500 m; shallower clouds produced lower drizzle rates. A similar conclusion regarding high drizzle frequency was reached by Fox and Illingworth (1997) based on in situ observations in stratocumulus around the Azores and around the British Isles. Our data confirm, with some qualifications, their finding that the 95-GHz reflectivity is dominated in stratus and stratocumulus by drizzle drops in spite of the minor contribution they make to LWC. As shown in our Fig. 6 for the three cases here described, the reflectivity from cloud droplets exceeded that due to drizzle drops only in the upper 50–150 m of the clouds.

Comparing the three cases of this paper, we find fairly similar characteristics with respect to cloud and drizzle drop populations. Total cloud droplet concentration was lowest on the first day; this may have been a reflection of depletion rather than of airmass origin. The cloud and drizzle drop size distributions were nearly identical (Fig. 17), except for the puzzling increase of the concentrations of smallest droplets with altitude on 14 September. Maximum drizzle drop sizes were 300-μm diameter on all 3 days. The basic characteristics of the profiles of drizzle concentrations (Fig. 17), reflectivities (Fig. 6), and correlations with air velocity (Fig. 9) are also invariant from day to day. Median drizzle rates near cloud base were approximately 0.01 mm h^{-1} for all 3 days and decreased by about a factor 5 toward cloud top. Maximum values for 1-s (90-m) averages of the drizzle rate were in the range 0.1–0.2 mm h^{-1}. The mass concentration of drizzle drops had median values of 5–8 $\times$ 10^{-3} g m^{-3} at cloud base, and decreased upward in a manner similar to the drizzle rate. The 1-s values for both drizzle rate and mass concentration show large scatter due to the small sample volume of the 2D-C probe. A better estimate of the variability in drizzle rate can be obtained from the reflectivity statistics shown in Fig. 7 using the unity exponent for the Z–R relationship quoted in section 5.

The size distribution of drizzle drops remains somewhat uncertain in this work due to the instrumentation problems mentioned in section 2. We appear to share this problem with others who use similar instruments; for example, the spectra obtained by Boers et al. (1996) show the same inflection near 50-μm diameter as our data. That this is not necessarily an artifact is given some support by the relatively good match between calculated and measured spectra obtained by Austin et al. (1995).

c. Upward transport of drizzle drops

Perhaps the most significant result emerging from our observations is the observed positive correlation between radar reflectivity and Doppler velocity (negative for downward velocities) in the upper regions of the clouds. This reversal from the negative correlation expected, and found, in the lower cloud regions and below the clouds, as well as the correlations found between in situ measurements of air velocity and drizzle drop concentration and mass, indicate an upward transport of drizzle drops through most of the depth of the cloud layer. The upward drizzle flux appears to be strongest near the middle of the cloud layer. Areas of upward transport (higher reflectivities) appear to have a broad range of horizontal extents and have irregular shapes. The radar data indicate the existence of regions of upward transport down to scales of 4 m; the supporting evidence derived from the in situ data is valid for scales down to about 90 m. At this time we are unable to deduce greater detail about the spectral characteristics of the flux, or to reliably estimate its total magnitude.

It may be noted that Hudson and Li (1995) found no correlation between vertical velocity and drizzle drop mass in two rather different cases of stratocumulus. This conflict is surprising because results from the two datasets are quite similar on several other points: positive correlations between vertical velocity and cloud droplet concentrations, negative correlations with average droplet size, and no correlations with cloud LWC. Possible reasons for the difference are that lower LWC was found in the cases observed by Hudson and Li (1995), and that their determination of drizzle mass relied on in situ probes only.

d. Cellular structure

The radar images (Figs. 4 and 5) show that apparently homogeneous stratus layers can have significant cellular

structures and that this structure is present in quite similar forms from case to case, in spite of significant differences in stability and wind conditions. The dominant horizontal scales of the cells were somewhat greater than the depths of the cloud layers, but were only about half of the depths of the total boundary layer for the 3 days analyzed. Horizontal sections of the cells (Fig. 5) reveal intricate shapes, tending toward fluted rather than lobed boundaries of the high reflectivity cores. There is some suggestion for wave organization on one day (14 September; Fig. 5a), but this evidence is not strong. No linear organization can be noted on the other days.

The cellular structure here reported has some resemblance to the finescale structure of the echoes described by Miller and Albrecht (1995). However, those data originated from a situation in which cumulus were interacting with stratocumulus, and which produced updrafts and rainfall rates an order of magnitude greater than those described in this paper. The ''microcells'' described by Kropfli and Orr (1993) were isolated, long lived, and had definite updraft cores. There is also some similarity with the echo cells described in Vali et al. (1995); weak convective buoyancy was believed to have been the driving force in that case. Nicholls (1989) diagnosed vertically coherent downdraft regions in stratus, and linked that observation to the cellular visual appearance of the cloud sheets. Furthermore, he determined the widths and frequencies of the downdraft regions as a function of distance below cloud top and showed that the observations can be matched to model simulations of a random traverse through hexagonal cells with a spacing of 0.6 times the depth of the mixed layer and with gaps between them 0.2 times the cell size. Downdraft occupied 40% of the area near cloud top and about half that near cloud base.

The spacing of echo cells in our cases (cf. section 9) are comparable to the thickness of the cloud layer. Since the cloud layers were 1.0, 0.47, and 0.55 times the depths of the mixed layers for the 3 days, the cell sizes in our cases are larger than those diagnosed by Nicholls (1989). Also, although we did not determine the fraction of area occupied by downdrafts, it is clear from Figs. 10 and 11 that near cloud top this number would be considerably smaller than the 40% given by Nicholls (1989). The main difference between the two sets of data is in cloud top instability, as will be discussed later. The diluted regions identified in Fig. 10 tend to change little in horizontal extent at first, then spread rapidly some distance away from the cloud top; this pattern has a degree of qualitative agreement with the observations of Nicholls (1989).

The observed pattern in radar echoes reflects the distribution of drizzle drops. In all cases and at all altitudes the pattern is dominated by drops >30 μm diameter; in the lower parts of the clouds that size shifts to 150–200 μm. Reflectivity values range over roughly 10 dBZ at given altitudes. As shown in section 5, reflectivity and precipitation flux are roughly proportional in these clouds, so that the echo patterns can be viewed as directly representing the distribution of drizzle intensity. How the uneven distribution of drizzle depends on and in turn influences other characteristics such as radiative fluxes, cloud breakup, thermal perturbations, etc., is clearly an important question.

The origin of the cellular echo patterns cannot be ascertained from the data on hand. It is especially intriguing that for the three cases studied the internal structures are qualitatively quite similar in spite of rather different dynamical conditions of the clouds. It is possible that wind shear at cloud top or gravity waves above the inversion were the common cause of the cellular structures. Another possibility is that weak buoyant fluxes on the last two days and disturbances induced by wind shear below the cloud on the first day (14 September) had comparable effects, though this would appear to be too much of a coincidence. Yet a third possibility is that positive feedback through the drag of the larger drops reinforces initially small variations in the growth rate or concentration of drizzle drops. The broader question of the origin of TKE in these clouds is clearly also relevant to the cellular organization—this point is taken up next.

e. Turbulence and entrainment

Since our data were not collected with turbulence studies in mind, only limited conclusions are warranted on this point. With that caveat, we venture into some speculations about the principal source of energy and hence the controlling factor for the observed turbulence, principally in order to examine relationships to the cellular echo structure.

For cloud situations that were in many ways similar to those here described, Nicholls and Leighton (1986) concluded that turbulence was maintained by radiatively driven convection from cloud top. Two ''signatures'' supporting that deduction were that the mixed layers did not extend all the way from cloud top to the surface, and the particular forms of the profiles of var(w) and of skew(w). We can compare our data with theirs on these two points. In our cases too, neutral stratification prevailed within the cloud layers. On one day (15 September) the mixed layer extended to the sea surface, whereas the other two days had more complex stratification below the cloud. The var(w) profiles shown in Fig. 18 are very similar to those of Nicholls and Leighton, and the skew(w) is negative within the cloud layer in both sets of data. This pattern also agrees with that reported by Moyer and Young (1991) for their flight B from the FIRE project, and with that of Frisch et al. (1995). In the latter report, we can compare with the statistics given for the Doppler velocity, since drizzle was negligible in their cases and therefore $V \approx w$. It thus appears that the var(w) and skew(w) profiles are quite robust features of stratus and of stratocumulus. In all, we believe that sufficient similarities exist between

our cases and those of Nicholls and Leighton and of Moyer and Young to apply their conclusions about the importance of radiative cooling in producing turbulence to the clouds we observed. However, there are also important differences between our cases and those of Nicholls and Leighton: there was little wind shear across the inversion, and drier air capped the clouds in their cases. The wind shear across the inversion was between 0.06 and 0.08 s^{-1} (over 80–100-m height intervals) in our cases, with Richardson numbers around 0.3; this raises the possibility that shear-induced turbulence was also an important factor. In addition to shear at the inversion, shear was also present in the stable layer below the cloud on 14 September (like in flight 564 of Nicholls and Leighton). With respect to the changes across the inversion, positive θ_E jumps and small q jumps indicate that there was no thermodynamic instability at cloud top in the clouds we studied. Even the simplified instability condition $\Delta\theta_E < b\Delta q$ ($b = 0.57, \ldots, 1.7$), which is not considered very restrictive (cf. MacVean 1993; Duynkerke 1993), is not satisfied in any of the cases, since $\Delta\theta_E$ values range from $+8$ to $+10$ K and $\Delta q <$ 0.6 g kg^{-1}. Thus, the strength of entrainment was certainly much less in our cases. In all, indications are that turbulence induced by evaporative cooling had a smaller role in these clouds than that derived from shear forces.

We do have evidence, in the radar images and in several aspects of the in situ measurements, that entrainment was taking place. The radar data of Fig. 10 show diluted parcels with relatively large downward velocities. In situ observations consistent with entrainment include (i) reduced values of LWC and increased values of var(LWC) near cloud top (Fig. 14), (ii) positive correlations near cloud top between w and Z_{calc} (Fig. 9), and between w and other parameters (Table 4), and (iii) traces showing downward moving air of reduced hydrometeor content (Fig. 11).

The diluted regions detected in this work are compatible in most respects with those described by Rogers and Telford (1986), Khalsa (1993), Wang and Albrecht (1994), and by Gerber (1996) among others. It is to be noted though, that these similarities exist even though thermodynamic entrainment instability was present in the comparison cases while our cases had none.

11. Conclusions

Observations were made in stratus over the upwelling zone off the Oregon coast with an aircraft equipped with in situ sensors and a 95-GHz radar. Measurements for three consecutive days were presented in this paper. Thermal stratification and wind conditions changed significantly during that period thus allowing differences and similarities to be exploited in search of underlying causes. The clouds were unbroken, with no detectable horizontal structure in parameters other than drizzle.

The observations here reported provide essentially a ''frozen'' description of cloud structure, in images and in statistical parameters. In situ measurements, taken along lines through the clouds, were extended by the radar data to horizontal and vertical planes. Conversely, the reflectivity and velocity fields detected by the radar were interpreted in light of the air motion and drop size distribution data from the in situ probes. In other words, the radar data provided a greater wealth of information than the in situ measurements along a line, and the ambiguities of reflectivity measurements were significantly reduced with the help of the simultaneous in situ measurements. Such combined data overcomes many of the problems and limitations identified, for example, by Davis et al. (1996) in the use of LWC data for examining scales of variation in stratocumulus.

The observations we report are consistent, in a general sense, with the model, also suggested by other authors, of broad regions of net upward fluxes and narrow entrainment regions of stronger downward motions. Our data refine this model in three respects. First, we show that the upward flux is most significant for drizzle drops over the size range 50–300-μm diameter, not for LWC made up by smaller cloud droplets. This difference has important implications regarding the way the upward transport is envisaged to come about, and certainly lessens the applicability of parallels between stratus and cumulus. Second, it is clear from the radar images that the regions of upward transport have irregular shapes over a large range of sizes. Third, we show that downward moving diluted regions existed in the clouds we examined, in spite of the absence of thermodynamic instability at cloud top. Especially in one case, and to lesser degrees in the other two, turbulence generated by wind shear might have been responsible for the initiation of entrainment.

Structures revealed by the kinds of radar echoes shown in this paper appear to provide a good basis for examining the degree and the scales of variability of drizzle in stratus and stratocumulus. The reflectivity images are nearly equivalent to images of precipitation concentration. It is clear that, through the many ways that drizzle interacts with other cloud properties, local variations in drizzle have significant impacts on a broad range of cloud characteristics and are of importance for the time evolution of the cloud. On the other hand, since drizzle represents a small fraction of the total water content of the cloud, effects of the drizzle structure are not felt in the instantaneous values of properties like liquid water path (LWP) or albedo.

Although we find the results presented here to be solidly supported by our data, undoubtedly these observations need to be confirmed, and their range of validity delineated, by cases from a broader range of conditions. The conclusions drawn need elaboration and integration in model simulations both with respect to dynamical and microphysical factors. At the same time, these observations might be helpful in providing ideas and realistic constraints to model calculations.

Acknowledgments. This work is part of a broader program for the acquisition and cloud physics application of the airborne millimeter-wave radar funded by National Science Foundation Grants ATM 9319907 and 9320672 to the University of Massachusetts—Amherst and the University of Wyoming (Dr. Ronald. C. Taylor program director), and by a DEPSCOR grant from the Office of Naval Research to the University of Wyoming. The outstanding support of all members of the University of Wyoming King Air Flight Facility was an indispensable part of this work. Special appreciation is due to E. Gasaway, L. V. Irving, G. G. Gordon, and L. Oolman, who participated in the field experiments. We also thank Prof. A. Rodi for help with several aspects of the air motion and other analyses. We sincerely thank Dr. Mark Miller and two other reviewers for their comments and suggestions.

REFERENCES

Austin, P. H., Y. Wang, R. Pincus, and V. Kujala, 1995: Precipitation in stratocumulus clouds: Observation and modeling results. *J. Atmos. Sci.,* **52,** 2329–2352.

Baker, M. B., 1993: Variability in concentrations of cloud condensation nuclei in the marine cloud-topped boundary layer. *Tellus Ser. B—Chem. Phys. Meteor.,* **45,** 458–472.

Baumgardner, D., and A. Korolev, 1997: Airspeed corrections for optical array probe sample volumes. *J. Atmos. Oceanic Technol.,* **14,** 1224–1229.

Boers, R., J. D. Spinhirne, and W. D. Hart, 1988: Lidar observation of the fine-scale variability of marine stratocumulus clouds. *J. Appl. Meteor.,* **27,** 797–810.

——, J. B. Jensen, P. B. Krummel, and H. Gerber, 1996: Microphysical and short-wave radiative structure of wintertime stratocumulus clouds over the Southern Ocean. *Quart. J. Roy. Meteor. Soc.,* **122,** 1307–1339.

Brenguier, J. L., 1989: Coincidence and dead-time corrections for particle counters. Part II: High concentration measurements with an FSSP. *J. Atmos. Oceanic Technol.,* **6,** 585–598.

——, and L. Amodei, 1989: Coincidence and dead-time corrections for particle counters. Part I: A general mathematical formalism. *J. Atmos. Oceanic Technol.,* **6,** 575–584.

Bretherton, C. S., and R. Pincus, 1995: Cloudiness and marine boundary layer dynamics in the ASTEX Lagrangian experiments. Part I: Synoptic setting and vertical structure. *J. Atmos. Sci.,* **52,** 2707–2723.

Browning, K. A., and Coauthors, 1993: The GEWEX Cloud System Study (GCSS). *Bull. Amer. Meteor. Soc.,* **74,** 387–399.

Cahalan, R. F., and J. B. Snider, 1989: Marine stratocumulus structure. *Remote Sens. Environ.,* **28,** 95–107.

——, W. Ridgeway, Wiscombe, W. J., T. L. Bell, and J. B. Snider, 1994: The albedo of fractal stratocumulus clouds. *J. Atmos. Sci.,* **51,** 2434–2455.

Clothiaux, E. E., M. A. Miller, B. A. Albrecht, T. P. Ackerman, J. Verlinde, D. M. Babb, R. M. Peters, and W. J. Syrett, 1995: An evaluation of a 94-GHz radar for remote sensing of cloud properties. *J. Atmos. Oceanic Technol.,* **12,** 201–229.

Davis, A., A. Marshak, W. Wiscombe, and R. Cahalan, 1996: Scale invariance of liquid water distributions in marine stratocumulus. Part I: Spectral properties and stationarity issues. *J. Atmos. Sci.,* **53,** 1538–1558.

Duroure, C., and B. Guillemet, 1990: Analyse des hétérogénéités spatiales des stratocumulus et cumulus. *Atmos. Res.,* **25,** 331–350.

Duynkerke, P. G., 1993: The stability of cloud top with regard to entrainment - amendment of the theory of cloud-top entrainment instability. *J. Atmos. Sci.,* **50,** 495–502.

Fabry, F., 1996: On the determination of scale ranges for precipitation fields. *J. Geophys. Res.-Atmos.,* **101,** 12 819–12 826.

Feingold, G., B. Stevens, W. R. Cotton, and A. S. Frisch, 1996: The relationship between drop in-cloud residence time and drizzle production in numerically simulated stratocumulus clouds. *J. Atmos. Sci.,* **53,** 1108–1122.

Fox, N. I., and A. J. Illingworth, 1997: The retrieval of stratocumulus cloud properties by ground-based cloud radar. *J. Appl. Meteor.,* **36,** 485–492.

Frisch, A. S., C. W. Fairall, and J. B. Snider, 1995: Measurement of stratus cloud and drizzle parameters in ASTEX with a K-alpha-band Doppler radar and a microwave radiometer. *J. Atmos. Sci.,* **52,** 2788–2799.

Galloway, J., A. Pazmany, R. McIntosh, R. Kelly, and G. Vali, 1996: MM-wave airborne cloud radars. *Proc. Remote Sensing: A Valuable Source of Information,* Toulouse, France, Advisory Group for Aerospace Research and Development, Publ. CP-582, 5.1–5.9.

Gerber, H., 1996: Microphysics of marine stratocumulus clouds with two drizzle modes. *J. Atmos. Sci.,* **53,** 1649–1662.

——, S. Chang, and T. Holt, 1989: Evolution of a marine boundary layer jet. *J. Atmos. Sci.,* **46,** 1312–1326.

Gollmer, S. M., Harshvardhan, R. F. Cahalan, and J. B. Snider, 1995: Windowed and wavelet analysis of marine stratocumulus cloud inhomogeneity. *J. Atmos. Sci.,* **52,** 3013–3030.

Hudson, J. G., and H. G. Li, 1995: Microphysical contrasts in Atlantic stratus. *J. Atmos. Sci.,* **52,** 3031–3040.

IGPO, 1994: Utility and feasibility of a cloud profiling radar. Publ. 10, International GEWEX Project Office, 53 pp.

Khalsa, S. J., 1993: Direct sampling of entrainment events in a marine stratocumulus layer. *J. Atmos. Sci.,* **50,** 1734–1750.

Kikuchi, K., M. Fulii, R. Shirooka, and S. Yoshida, 1991: The cloud base structure of stratocumulus clouds. *J. Meteor. Soc. Japan,* **69,** 701–708.

——, Y. Asuma, T. Taniguchi, M. Kanno, M. Tanaka, T. Hayasaka, T. Takeda, and Y. Fujiyoshi, 1993: Structure and reflectence of winter maritime stratocumulus clouds. *J. Meteor. Soc. Japan,* **71,** 715–731.

Kogan, Y. L., M. P. Khairoutdinov, D. K. Lilly, Z. N. Kogan, and Q. F. Liu, 1995: Modeling of stratocumulus cloud layers in a large eddy simulation model with explicit microphysics. *J. Atmos. Sci,* **52,** 2923–2940.

Kropfli, R. A., and B. W. Orr, 1993: Observations of microcells in the marine boundary layer with 8-mm wavelength Doppler radar. Preprints, *26th Int. Conf. on Radar Meteorology,* Norman, Oklahoma. Amer. Meteor. Soc., 492–494.

——, S. Y. Matrosov, T. Uttal, B. W. Orr, A. S. Frisch, K. A. Clark, B. W. Bartram, R. F. Reinking, J. B. Snider, and B. E. Martner, 1995: Cloud physics studies with 8 mm wavelength radar. *Atmos. Res.,* **35,** 299–313.

Krueger, S. K., G. T. Mclean, and Q. Fu, 1995a: Numerical simulation of the stratus-to-cumulus transition in the subtropical marine boundary layer. Part I: Boundary-layer structure. *J. Atmos. Sci.,* **52,** 2839–2850.

——, ——, and ——, 1995b: Numerical simulation of the stratus-to-cumulus transition in the subtropical marine boundary layer. Part II: Boundary-layer circulation. *J. Atmos. Sci.,* **52,** 2851–2868.

Lee, J., J. Chou, R. C. Weger, and R. M. Welch, 1994: Clustering, randomness, and regularity in cloud fields. 4. Stratocumulus cloud fields. *J. Geophys. Res.-Atmos.,* **99,** 14 461–14 480.

Leon, D., and G. Vali, 1998: Retrieval of three-dimensional particle velocity from airborne Doppler radar data. *J. Atmos. Oceanic Technol.,* **15,** 860–870.

Lhermitte, R. M., 1988a: Cloud and precipitation remote sensing at 94 GHz. *IEEE Trans. Geosci. Remote Sens.,* **26,** 207–216.

——, 1988b: Observation of rain at vertical incidence with a 94 GHZ

Doppler radar: An insight on Mie scattering. *Geophys. Res. Lett.*, **15,** 1125–1128.

——, 1990: Attenuation and scattering of millimeter wavelength radiation by clouds and precipitation. *J. Atmos. Oceanic Technol.*, **7,** 464–479.

Liebe, H. J., T. Manabe, and G. A. Hufford, 1989: Millimeter-wave attenuation and delay rates due fog/cloud conditions. *IEEE Trans. Antenn. Prop.,* **37,** 1617–1623.

MacVean, M. K., 1993: A numerical investigation of the criterion for cloud-top entrainment instability. *J. Atmos. Sci.,* **50,** 2481–2495.

Mead, J. B., A. L. Pazmany, S. M. Sekelsky, and R. E. McIntosh, 1994: Millimeter-wave radars for remotely sensing clouds and precipitation. *Proc. IEEE,* **82,** 1891–1906.

Miller, M. A., and B. A. Albrecht, 1995: Surface-based observations of mesoscale cumulus-stratocumulus interaction during ASTEX. *J. Atmos. Sci.,* **52,** 2809–2826.

Moyer, K. A., and G. S. Young, 1991: Observations of vertical velocity skewness within the marine stratocumulus-topped boundary layer. *J. Atmos. Sci.,* **48,** 403–410.

Nicholls, S., 1987: A model of drizzle growth in warm, turbulent, stratiform clouds. *Quart. J. Roy. Meteor. Soc.,* **113,** 1141–1170.

——, 1989: The structure of radiatively driven convection in stratocumulus. *Quart. J. Roy. Meteor. Soc.,* **115,** 487–511.

——, and J. Leighton, 1986: An observational study of the structure of stratiform cloud sheets. Part I: Structure. *Quart. J. Roy. Meteor. Soc.,* **112,** 431–460.

Paluch, I. R., and D. H. Lenschow, 1991: Stratiform cloud formation in the marine boundary layer. *J. Atmos. Sci.,* **48,** 2141–2158.

——, C. A. Knight, and L. J. Miller, 1996: Cloud liquid water and radar reflectivity of nonprecipitating cumulus clouds. *J. Atmos. Sci.,* **53,** 1587–1603.

Pazmany, A., J. Mead, R. Mcintosh, M. Hervig, R. Kelly, and G. Vali, 1994a: 95-GHz polarimetric radar measurements of orographic cap clouds. *J. Atmos. Oceanic Technol.,* **11,** 140–153.

——, R. E. McIntosh, R. D. Kelly, and G. Vali, 1994b: An airborne 95 GHz dual-polarized radar for cloud studies. *IEEE Trans. Geosci. Remote Sens.,* **32,** 731–739.

Rogers, D. P., and J. W. Telford, 1986: Metastable stratus tops. *Quart. J. Roy. Meteor. Soc.,* **112,** 481–500.

Sassen, K., and L. Liao, 1996: Estimation of cloud content by W-band radar. *J. Appl. Meteor.,* **35,** 932–938.

Sauvageot, H., 1976: Circulation de l'air et formation des précipitations dans les stratocumulus en rouleaux. *J. Rech. Atmos.,* **10,** 17–24.

Schubert, W. H., J. S. Wakefield, E. J. Steiner, and S. K. Cox, 1979: Marine stratocumulus convection. Part I: Governing equations and horizontally homogeneous solutions. *J. Atmos. Sci.,* **36,** 1286–1307.

Vali, G., R. D. Kelly, A. Pazmany, and R. E. Mcintosh, 1995: Airborne radar and in-situ observations of a shallow stratus with drizzle. *Atmos. Res.,* **38,** 361–380.

Wang, Q., and B. A. Albrecht, 1994: Observations of cloud-top entrainment in marine stratocumulus clouds. *J. Atmos. Sci.,* **51,** 1530–1547.

Welch, R. M., K. S. Kuo, B. A. Wielicki, S. K. Sengupta, and L. Parker, 1988a: Marine stratocumulus cloud fields off the coast of Southern California observed using LANDSAT imagery. Part I: Structural characteristics. *J. Appl. Meteor.,* **27,** 341–362.

——, S. K. Sengupta, and K. S. Kuo, 1988b: Marine stratocumulus cloud fields off the coast of Southern California observed using LANDSAT imagery. Part II: Textural analysis. *J. Appl. Meteor.,* **27,** 363–378.

White, A. B., C. W. Fairall, A. S. Frisch, B. W. Orr, and J. B. Snider, 1996: Recent radar measurements of turbulence and microphysical parameters in marine boundary layer clouds. *Atmos. Res.,* **40,** 177–221.